RESEARCH REPORTS

OF THE

FACULTY OF ENGINEERING

MIE UNIVERSITY

Vol. 30

December 2005

PUBLISHED BY
FACULTY OF ENGINEERING
MIE UNIVERSITY
TSU, MIE, JAPAN

三重大学工学部研究報告
第３０巻　　２００５年１２月

目　　次

論文

劉　宇，小野喜央，松村忠朗,平野　敦,市川貴之,今西誠之,武田保雄：
固体高分子電解質とインターカレーション電極を主体とした全固体
リチウムイオン電池 …… 1

論文（和文）

小竹茂夫：
フレッシュマンに贈る量子計算の概略と基礎…… １３

博士論文梗概（２００４年度 博士(工学）の学位取得者）…… ３８

論文抄録（２００４年掲載） ……Ａ－１

著書・編書・訳書・総説抄録（２００４年発行および掲載） ……Ａ－５６

三　重　大　学
工学部研究報告
平成17年12月1日発行

編集兼発行者　三重大学工学部
三重県津市栗真町屋町1577

Research Reports of the Faculty of Engineering
Mie University
Vol.30 December 2005

CONTENTS

Original Papers

Y. Liu, Y.Ono, T. Matsumura, A. Hirano, T. Ichikawa, N. Imanishi and Y. Takeda:
All solid-state Li-ion batteries based on intercalation electrodes and poly (ethylene oxide)-LiX electrolytes 1

Original Papers(Japanese)

Sigeo Kotake:
Concept and Images of Quantum Computation for Freshmen
- Basic summery of Quantum computation - 13

Abstracts of Doctor's Theses (Received The Degree of Doctor of Engineering in 2004) 38

Abstracts of Papers (Published in 2004) A-1

Abstracts of Books and Reviews (Published in 2004) A-56

Research Reports of the Faculty of Engineering, Mie University

Faculty of Engineering,Mie University
1577 Kurimamachiya-cho,Tsu,Mie 514-8507 JAPAN

Original Paper

All solid-state Li-ion batteries based on intercalation electrodes and poly (ethylene oxide)-LiX electrolytes

Y. Liu[a], Y.Ono[b], T. Matsumura[b], A. Hirano[b], T. Ichikawa[b], N. Imanishi[b] and Y. Takeda[b]
([a] Satellite Venture Business Laboratory, [b] Department of Chemistry for Materials)

(Received September 20, 2005)

Abstract
All-solid state rechargeable Li-ion batteries based on poly (ethylene oxide) electrolytes are promising power sources for large application such as electric vehicles (EV), which could be likely to require safety and reliability as well as high energy density and long cycle life. However, so far, state-of-the-art electrode materials are limited by the performance factors such as electrochemical instability to lithium insertion/extraction, particularly at the solid/solid interface between the electrodes and the PEO electrolytes. The efforts on conquering above dilemma have been carried out over several decades. Recently, we developed novel or modified insertion type electrodes, which demonstrate good electrochemical behavior with the PEO electrolytes at the elevated temperature. In this paper, preparation and characterization of the electrodes proposed are presented and discussed in detail.

Key words: Power sources; Rechargeable lithium ion batteries; All solid-state PEO electrolytes; Insertion electrodes; Energy density; Thermal safety.

1. Introduction

Solid-state rechargeable batteries, especially, lithium ion batteries, are principle and promising power sources for a wide variety of electronics. PEO electrolyte formed by dissolving a lithium salt in a host poly (ethylene oxide) (PEO) shows high ionic conductivity ($\sigma > 10^{-4}$ S cm^{-1}) at the elevated temperature. Rechargeable lithium batteries based on the PEO electrolytes have been proposed to overcome low energy density of previously used batteries such as lead acid and nickel metal hydride and to improve safety of conventional lithium-ion batteries with an inflammable liquid electrolyte [1]. The PEO type cells have several benefits such as feasible design and ductile morphology which can absorb volume change for Li insertion/extraction in electrodes. Although the high temperature limitation (>60 ℃) of the PEO cell is a drawback for applications in the consumer electronic market, it is probably an advantage for numerous other applications such as for electric vehicles (EV). For these large size batteries in EV, safety and reliability are the most important issues. Previously developed lithium polymer batteries contain lithium metal anodes. A lithium battery incident at Los Angeles International Airport on 28 April, 1999 suggests that safety of a lithium battery with a large amount of lithium metal is questionable [2]. In addition, an improvement on the ionic conductivity and Li^+ transfer number has to be done to achieve a relatively high charge rate. Therefore, so far, research has been extensively concentrated on two major points such as 1) the improvement of ionic conductivity of PEO-LiX complex at the relatively low temperature and 2) searching for novel or modified electrodes which can deliver good interfacial compatibility with the solid PEO electrolytes. By this motivation, in the anode side, researchers have undertaken to replace the lithium metal by a safer one, such as insertion anode, with a high capacity and an excellent reversibility. Lithium-insertion hosts such as carbon, Li-alloy and Li-M-O are promising alternative anodes [3, 4]. Unfortunately, carbon still cannot be adopted successfully with the PEO electrolytes due to the interfacial incompatibility, regardless of its wonderful electrochemical manners in the liquid system. On the other hand, some Li-M-O materials, e.g., spinel $Li_4Ti_5O_{12}$, demonstrate zero-strain effects for Li-insertion, resulting in long cycling life with the solid PEO electrolytes. However, relatively low capacity and high Li reactive potentials of lithium titanates make them incomparable in the energy density. On the other hand, in the cathode side, the most common cathodes such as $LiCoO_2$, $LiNiO_2$, $LiCo_xNi_{1-x}O_2$, and $LiMn_2O_4$ all suffer from side reaction with PEO electrolytes and detrimental phase transitions above 70 ℃ that inevitably cause to capacity loss and fade while being oxidized at a high potential. Meanwhile, state-of-the-art electrode materials are limited by the performance factors such as electrochemical instability to

lithium insertion/extraction, particularly at the interface between the electrodes and the PEO electrolytes. Therefore, development in the electrode materials in associated with the PEO electrolytes would be urgent.

2. Experimental

2.1 Materials preparations

To produce the hexagonal lithium transition-metal nitrides, a given ratio of Li_3N and powders of transition metals was homogeneously mixed in an Ar atmosphere. The mixture was pressed into a tablet with 8 mm in diameter and 5-8 mm in thickness and heated at 700℃ for 12 h under N_2 stream with heating rate of 35 ℃ min^{-1}. The reactions were allowed cool down to room temperature normally. For the compounds containing Fe, the heating temperature was increased to 800 ℃. The resulting products were ground in a glove box and further treated by high-energy mechanical milling (HEMM) at a rotational speed of 500 rpm for 20 h. The modification for the graphitic carbon was as follows: a given amount of graphitic carbon was dried under vacuum at high temperature, and then was mixed with metallic lithium and selected organic solvent under a certain ratio under inert atmosphere. The mixture was treated by high energy mechanical milling under inert atmosphere. The milled product was further dried under high temperature to entirely remove the residual organic solvent. Ultrafine SnSb alloy powder (particle size < 0.2 μm) was prepared by chemical precipitation from aqueous solutions containing the reductive agent $NaBH_4$ and respective metallic salts in the presence of complexants such as citrates. The Co_3O_4 powder (< 2 μm) was obtained by a thermal decomposition of $CoCO_3$ at 800 ℃ in air. $LiNi_{0.8}Co_{0.2}O_2$ (ca. 10 μm) was prepared from the mixture of Li_2O_2 (Aldrich) and $(Ni_{0.8}Co_{0.2})O$ precursor which was obtained from the decomposition of the hydroxide at 300 ℃ for 1 h. The mixture was heated at 700 ℃ for 24 h under O_2 gas flow. $LiFePO_4$ and $LiFePO_4$/C (PVC as carbon sources) was prepared as follows: a certain amount of Li_2CO_3, poly (vinyl chloride) (PVC), $NH_4H_2PO_4$ and FeC_2O_4 was homogeneously mixed by the aid of THF. The mixture was heated firstly at 350 ℃ for 3-6 h and smashed at room temperature. The smashed products were further heated at 700-900 ℃ for 16 h under Ar. The final samples were ground and sieved. Powder X-ray diffraction (XRD) patterns were obtained using automated powder diffractometer with Cu K_α radiation (Rotaflex RU-200B, Rigaku-denki Corporation). The morphological performance of the materials was characterized with scanning electron microscopy (SEM) and Electron Probe Micro-Analysis (EPMA).

2.2 PEO Electrolytes and cathode film

PEO electrolytes (Li/O ratio: 1/18) were prepared under a casting technique. All the procedure was protected by Ar atmosphere in the glove box. A given weight of PEO (MW = 6×10^5) and $LiN(CF_3SO_2)_2$ was dissolved completely in anhydrous acetonitrile (AN). $BaTiO_3$ (ca. 0.1 μm) was dispersed homogeneously in the solution as filler. After strong stirring overnight the viscous solution was cast into a Teflon dish. After AN was slowly and completely evaporated under a N_2 flow, the obtained film was further dried at 90 ℃ under vacuum at least 8 h. The conductivities of the composite polymer electrolyte were observed as high as $1.7x10^{-3}$ S cm^{-1} at 80 ℃ and $0.82x10^{-3}$ S cm^{-1} at 65 ℃ and the decomposition potential was estimated to be more than 4.2 V (vs. Li/Li^+). The cathode electrode consisting of 52 wt.% active hosts ($LiFePO_4$ or $LiNi_{0.8}Co_{0.2}O_2$), 10 wt.% acetylene black(AB) and 38 wt.% PEO-$LiN(CF_3SO_2)_2$ (Li/O ratio: 1/18) were prepared by the casting method similar to PEO film and the thickness was about 200 μm.

2.3 Anode preparations

For all the electrodes, a given weight of the electrode components was homogeneously mixed in an agate mortar in a glove box and further pressed onto a 300-mesh stainless steel grid, which served as a current collector. The geometric area of the electrodes was 0.55 cm^2, and the typical thickness was 100~160 μm.

2.4 Electrochemical and thermal stability (DSC) measurements

To evaluate the electrochemical properties of the electrodes, a half-cell containing Li metal as the counter and $LiPF_6$ / EC+DMC (Ethylene carbonate plus diethyl carbonate as 1:1 in volume) electrolytes (in case of the cells with the liquid electrolytes) was used. Basically all the three layers, including test electrode, separator and Li metal, were stacked in a 2025 coin type cell in a glove box. For the cells based on the PEO electrolyte, the separator was replaced by the PEO film, which also served as electrolyte. The full solid-state cell was constituted by replacing lithium metal with the cathode films. A small constant pressure was kept inside cells by means of the Ni foam as filler. Before the electrochemical test, the PEO based cells were preheated for 2 hrs at a temperature of 75℃. Unless stated elsewhere, the cells were carried out at a constant current density of 0.1-0.15 mA cm^{-2}. The rest time between charge and discharge was 1 min.

3. Results and discussion

3.1 Anodes

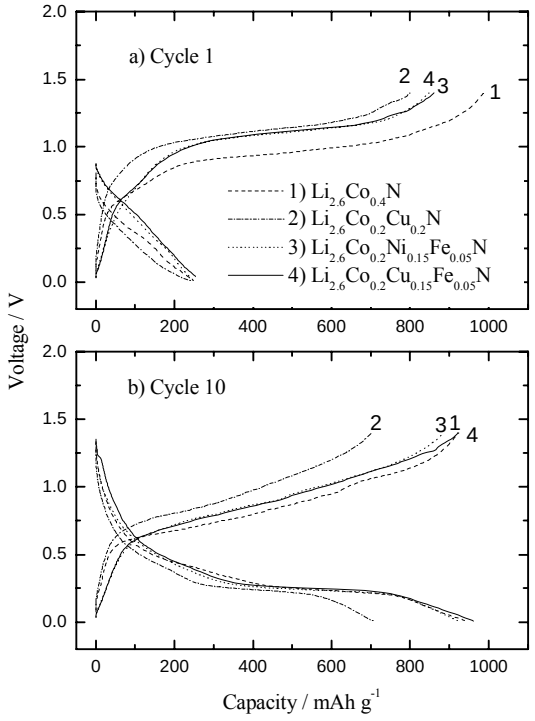

Fig.1. Charge and discharge curves of the electrodes based on lithium transition-metal nitrides at the first and tenth cycle, voltage cutoff: 0-1.4 V, vs. Li/Li^+. Electrode composition: 20 wt.% AB, 70 wt.% lithium metal nitrides and 10 wt.% PVDF.

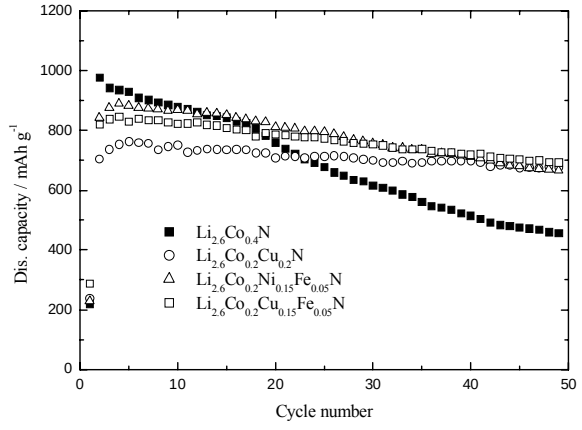

Fig.2. Cycling performance of the electrodes based on lithium transition-metal nitrides. Electrode compositions are the same as in Fig.1.

3.1.1 Electrochemical behavior and thermal stability of the composite electrodes.

Lithium metal (transition) nitrides with hexagonal symmetry, P6/*mmm*, are composed of M (M=Co, Cu, Ni) substituting lithium between the $Li_2^+N^{3-}$ layers of Li_3N [5,6]. Fig.1 shows the electrochemical behavior of the lithium transition-metal nitrides prepared from solid-state reaction and high-energy mechanical milling (HEMM). Due to the vacant sites introduced by the doped transition metals, the fully lithiated nitrides can still allow a small amount of lithium intercalation in the first cycle. The compounds gradually undergo an irreversible transformation from a crystalline phase to an amorphous one in the first Li-extraction stage, as shown in Fig.1a. Compared with $Li_{2.6}Co_{0.4}N$, the slight increase of the co-doped nitrides in the charge potentials indicates that part Co substituted by Cu, Ni and Fe may be obstructive to the lithium extraction [7,8]. In the subsequent cycle shown in Fig.1b, the charge potentials become slope and a large amount of lithium can be reversibly re-intercalated and extracted, resulting in high capacities of 700-950 mAh g^{-1} which are about 2-3 times over that of the commercial graphite. The discharge potential curves, on the other hand, demonstrate a hystersis of ca. 0.5 V compared with the charge ones, indicating the different electrochemical kinetics for Li intercalation and extraction. A comparison with $Li_{2.6}Co_{0.4}N$ in the cycling performance reveals that the co-doped compounds have a remarkably enhanced cyclability shown in Fig.2. The significant improvement in the cycling performance for the co-doped nitrides can be attributed to the improved structural stability in association with the Li extraction degree and the enhanced interfacial compatibility [7,8]. Lithium metal nitrides are very attractive in the packing density and volumetric capacity due to the density similar to the current graphite. A major hindrance to the nitrides as promising anode alternatives for graphite is that they possess Li-rich structure and therefore cannot directly combine with the typically high-potential cathodes such as $LiCoO_2$ and $LiMn_2O_4$ to constitute Li-ion cells. This deterrent can be overcome by introducing an appropriate amount of Co_3O_4 into the electrodes containing above lithium metal nitrides.

Fig.3 shows charge and discharge curves of the a) Co_3O_4, b) $Li_{2.6}Co_{0.2}Cu_{0.2}N$ and c) Co_3O_4-$Li_{2.6}Co_{0.2}Cu_{0.2}N$ based electrodes vs. lithium under a potential of 0-1.4 V with liquid electrolytes at room temperature. The Co_3O_4 electrode has a large insertion capacity of 1150 mAh g^{-1} along with a potential plateau of about 1.05 V in the first cycle. However, its capacity retention in the subsequent cycle shown in Fig.3a is below to 180 mAh g^{-1} under the potential range of

0-1.4V. This is attributed that this material has to be electrochemically activated under a very wide potential as 0-3 V [9]. The electrochemical behavior of the $Li_{2.6}Co_{0.2}Cu_{0.2}N$, which has a high extraction capacity as 800 mAh g^{-1} with a potential plateau of 1.0 V but an insertion capacity low as 230 $mAhg^{-1}$, is obviously in contrast to that of the Co_3O_4, as shown in Fig.3b. In the case of $Li_{2.6}Co_{0.2}Cu_{0.2}N$ plus Co_3O_4, a very high first charge recovery of ca. 100% shown in Fig3c is remarkable while the cycling is started from an insertion process. Moreover, the composite electrode does not show an obvious potential plateau in the charge stage that reflects the coexistence of two phases in the active hosts similar to that of the $Li_{2.6}Co_{0.2}Cu_{0.2}N$. Thus, it comes to conclusion that $Li_{2.6}Co_{0.2}Cu_{0.2}N$ in the composite electrode might be discharged from a delithiated or an amorphous state. The Li-intercalation potential of Co_3O_4 (ca.1.1V) is slightly higher than the Li-extraction potential of lithium metal nitride (ca.1.0V); therefore Co_3O_4 can thermodynamically extract lithium from the nitrides. XRD measurements confirm this point because lithium transfer into Co_3O_4 would be evidenced by a change in the peak intensities for both the hosts. We proposed the reaction mechanism of the composite electrode as follows: $Li_{2.6}Co_{0.2}Cu_{0.2}N + xCo_3O_4 \rightarrow Li_{2.6-8x}Co_{0.2}Cu_{0.2}N + 4xLi_2O + 3xCo$ (1)

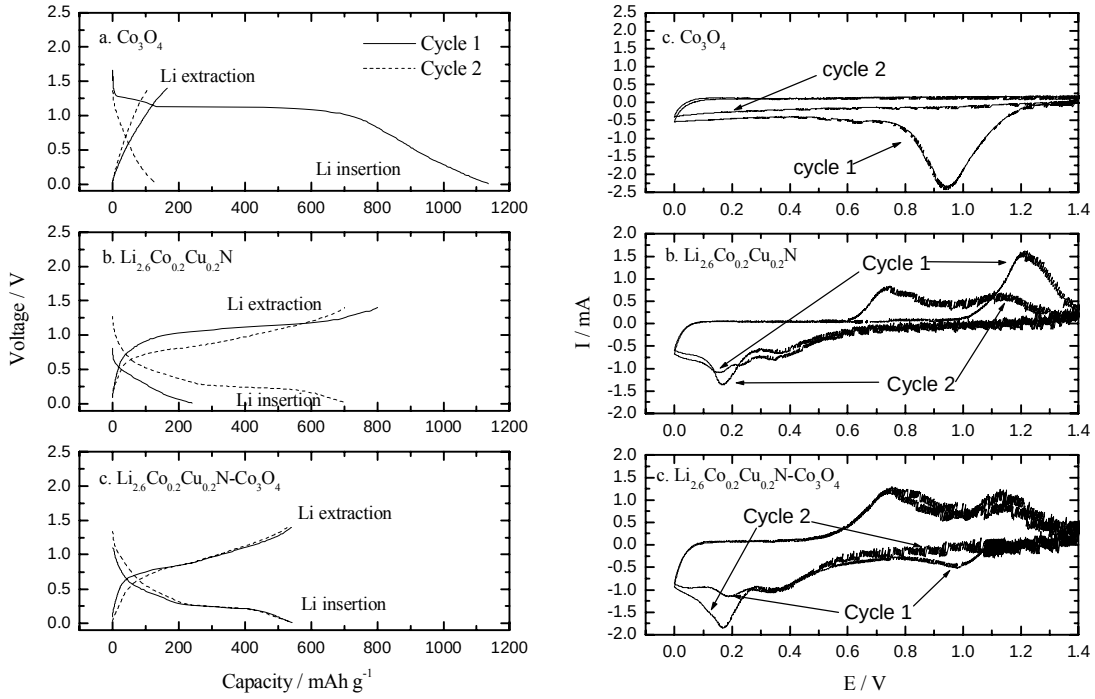

(Left) Fig.3. Charge and discharge curves of different cells based on a) Co_3O_4, b) $Li_{2.6}Co_{0.2}Cu_{0.2}N$ and c) Co_3O_4-$Li_{2.6}Co_{0.2}Cu_{0.2}N$, voltage cutoff: 0-1.4 V, vs. Li/Li^+. Electrode compositions: a) 80 wt.% Co_3O_4, 10 wt.% AB and 10 wt.% PVDF; b) 70 wt.% $Li_{2.6}Co_{0.2}Cu_{0.2}N$, 20 wt.% AB and 10 wt.% PVDF and c) 50 wt.% $Li_{2.6}Co_{0.2}Cu_{0.2}N$, 30 wt % Co_3O_4, 10 wt.% AB and 10 wt.% PVDF.
(Right) Fig.4. Cyclic voltammogram of the electrode based on a) Co_3O_4, b) $Li_{2.6}Co_{0.2}Cu_{0.2}N$ and c) Co_3O_4-$Li_{2.6}Co_{0.2}Cu_{0.2}N$ at the scan rate of 0.05 mV S^{-1}, voltage cutoff: 1.4-0. V, vs. Li/Li^+. Electrode composites are the same as in Fig.3.

$Li_{2.6-8x}Co_{0.2}Cu_{0.2}N + zLi^+ + ze^- = Li_{2.6-8x+z}Co_{0.2}Cu_{0.2}N$ (2).

Reaction (1) is a chemical reaction and reaction (2) is an electrochemical one. If $Li_{2.6-8x}Co_{0.2}Cu_{0.2}N$ is the composition of the fully charged state, then reaction (2) becomes reversible during charge and discharge even at the first cycle. From the experimental results shown in Fig. 3, we estimated x and z as 0.16 and 1.7, respectively. These values correspond to 60/40 weight ratio of $Li_{2.6-8x}Co_{0.2}Cu_{0.2}N/Co_3O_4$ and the reversible capacity of 477 mAh g^{-1}. The capacity was calculated by including $Li_{2.6-x}Co_{0.2}Cu_{0.2}N$ and Co_3O_4 as active hosts. We observed a first charge efficiency of 100% and a reversible capacity of ca. 520 mAh g^{-1} for the composite electrode containing of 62.5 wt. % $Li_{2.6-x}Co_{0.2}Cu_{0.2}N$ plus 37.5 wt % Co_3O_4, as shown in Fig. 3c. The high first cycle efficiency proposed can greatly extend the capacity utilization for the cathode. It is very remarkable because the low charge efficiency of the anodes in the first cycle might consume extra capacity from cathodes and thereby

inevitably reduce the total energy density of the cells. Cyclic voltammogram was further conducted on the electrodes based on different active hosts with a scan rate of 0.05 mV s^{-1} in the potential scale of 0-1.4 V vs. Li/Li^+, as shown in Fig.5. There is one cathodic peak at about 0.95 V in the first Li-insertion process for Co_3O_4 (Fig.4a. However, this peak does not repeat in the subsequent cycle, indicating that Co_3O_4 turns into inert to lithium. In the case of $Li_{2.6}Co_{0.2}Cu_{0.2}N$, an obvious anodic peak shown in Fig.4b appears at 1.2 V in the first cycle that corresponds to the two-phase transformation. In the subsequent cycle, one cathodic peak at 0.18 V and two anodic peaks at 0.78, 1.12 V become visible and remain to be stable. However, the large hystersis in the cathodic and anodic processes seems a drawback and has to be further conquered. In comparison with $Li_{2.6}Co_{0.2}Cu_{0.2}N$ and Co_3O_4, obviously, the behavior of the composite electrode shown in Fig.4c is highly consistent with that of $Li_{2.6}Co_{0.2}Cu_{0.2}N$, suggesting that the active host in the composite is mainly associated with lithium metal nitrides. Furthermore, a weak cathodic peak at 0.95 V corresponding to the Co_3O_4 indicates that the thermodynamically spontaneous reaction may not entirely drive lithium into the Co_3O_4 before the electrochemical cycling. The composite electrodes demonstrated high cycling stability, due to that they could be benefited from the low volume effects of the lithium metal nitrides upon Li insertion and extraction. As measurement, the charge yield of the composite electrode during cycling is always at 100%, indicating that Co_3O_4 remains inactive and stable in the electrode while lithium in the nitrides can be electrochemically intercalated and extracted with high reversibility under a suitable potential window. The composite electrode consisting of $Li_{2.6-x}Co_{0.2}Cu_{0.2}N$-$Co_3O_4$ was found to show good electrochemical behavior with the solid PEO electrolytes. A high charge efficiency of 99.6 % and a large capacity of 520 mAh g^{-1} shown in Fig.5 become feasible, indicating that lithium can be electrochemically

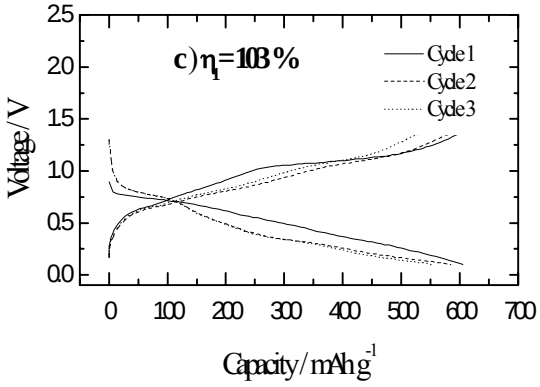

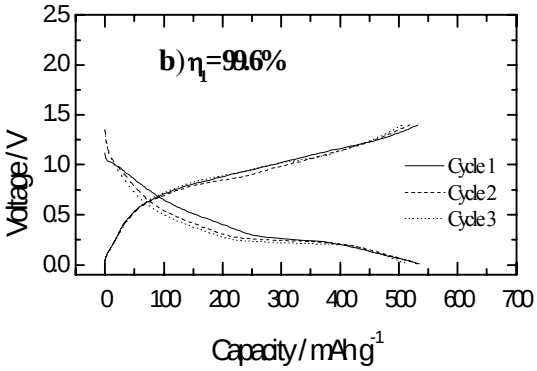

(Left) Fig.5. Charge and discharge profiles of the SnSb-$Li_{2.6}Co_{0.4}N$ electrode with PEO at 65 °C.
(Right) Fig.6. Charge and discharge profiles of the Co_3O_4-$Li_{2.6}Co_{0.2}Cu_{0.2}N$ electrode with PEO at 65 °C.

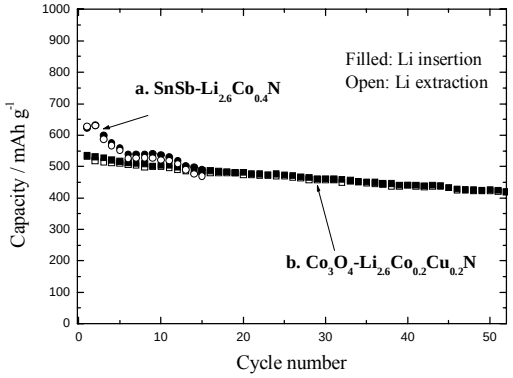

Fig.7. Cycling performance of the composite anodes with PEO electrolytes.

intercalated into and extracted from the nitrides with high reversibility while operating with the PEO electrolytes.

On the other hand, the composite electrode based on SnSb and $Li_{2.6}Co_{0.4}N$ also demonstrates a high first charge efficiency of 103 %, which is attributed to the fact that lithium metal nitrides can make a capacity compensation for the ultrafine alloy hosts in the first cycle [10]. As can be seen, the charge-discharge behavior of the SnSb-$Li_{2.6}Co_{0.4}N$ composite electrode reflects the mixing electrochemical characteristics of these two types of active hosts, as shown in Fig.6. The capacity changes, as a function of cycling, for different anodes with the solid PEO electrolytes are shown in Fig. 7. The SnSb-$Li_{2.6}Co_{0.4}N$ anode has a large capacity of over 600 mAh g^{-1} in the cycling beginning. However, a gradual deterioration in the cycling performance is always observed. A replacement of $Li_{2.6}Co_{0.4}N$ with the co-doped nitrides proposed does not bring any progress, indicating that the volume effect from the Li-alloying reaction possesses a morphological instability at the interface while operating with the solid-state PEO electrolytes.

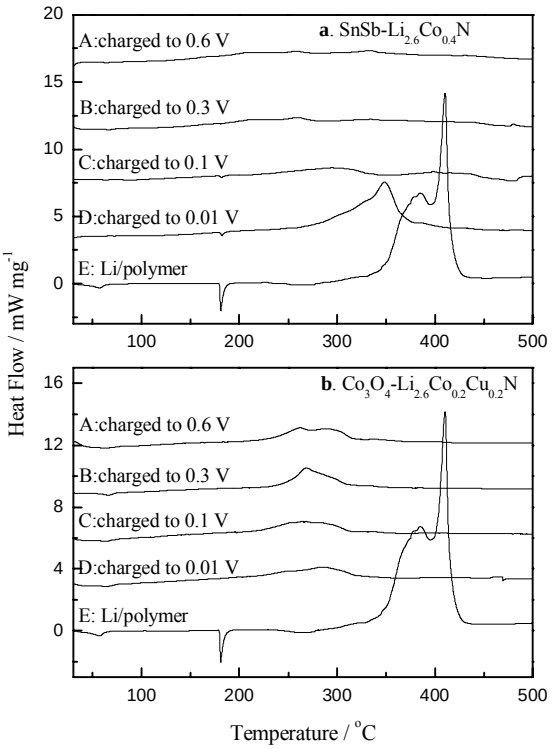

Fig.8. DSC curves of the composite anodes of a) SnSb-$Li_{2.6}Co_{0.4}N$ and b) $Li_{2.6}Co_{0.2}Cu_{0.2}N$-$Co_3O_4$ with various Li intercalation states (Heating rate: 5°C/min).

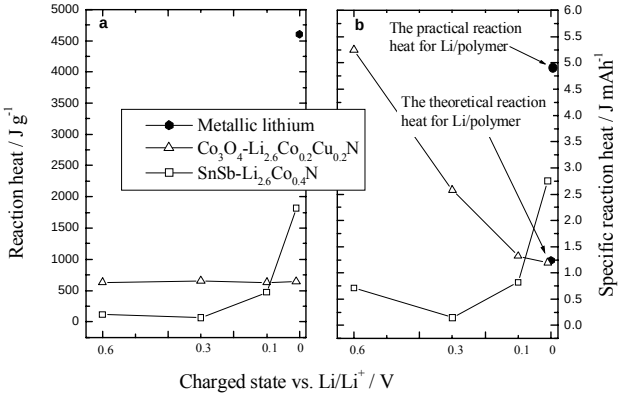

Fig.9. Reaction heat vs. charged state by a) J g^{-1} and b) J mAh^{-1} for different anodes at 65℃

By using the $Li_{2.6-x}Co_{0.2}Cu_{0.2}N$-$Co_3O_4$ anode, a significantly improved cycling performance was obtained with a high capacity of 500 mAh g^{-1}. The charge-discharge efficiency is almost 100% and the capacity fade during cycling is estimated to be only about 0.37%/cycle. The capacity retention can be further improved by decreasing moisture in the PEO electrolytes since hexagonal lithium metal nitrides suffer from a high sensitivity with H_2O.

The safety of small size lithium-ion cells under normal use is well established. In contrast, the safety of the large size lithium-ion batteries is still questionable, especially in cases of abusive use. Safety of lithium ion batteries is mainly related to the thermal reactivity of the components. Fig.8 shows differential scanning calorimetric curves (DSC) for the composite anodes of $Li_{2.6}Co_{0.4}N$-SnSb (a) and $Li_{2.6}Co_{0.2}Cu_{0.2}N$-$Co_3O_4$ (b) with the PEO electrolytes, respectively, as a function of the charged state along with that for Li metal with the PEO electrolytes (1:1 weight ratio) as a reference. For the $Li_{2.6}Co_{0.4}N$-SnSb anode, the reaction heat strongly depends on the charged state. The reaction heat is very low for the composite anode charged up to 0.3 V and appreciable for that charged up to 0.1 V, as shown in Fig.8a. An endothermic peak in the anode charged to 0.1 V is observed at 180°C in the DSC curve, which corresponds to the fusion of lithium metal. That is, the high level insertion of lithium into the $Li_{2.6}Co_{0.4}N$-SnSb composite exhibits a lithium metal deposition. On the other hand, the reaction heat of the $Li_{2.6}Co_{0.2}Cu_{0.2}N$-$Co_3O_4$ anode shows exothermic peaks at 250~320 °C, which do not depend on the charged state, as shown in Fi.8b. Fig.9 shows the reaction heat (a) and specific reaction heat (b) of the different anodes at various charged states. The reaction heat of the anode should be compared in terms of energy per discharged capacity, i.e., J mAh^{-1} (a specific reaction heat). Specific reaction heats for the $Li_{2.6}Co_{0.2}N$-SnSb anode charged up to 0.1V vs. Li/Li^+ and 0.01 V vs. Li/Li^+ are 0.82 J mAh^{-1} and 2.75 J mAh^{-1}, respectively. Those for the $Li_{2.6}Co_{0.2}Cu_{0.2}N$-$Co_3O_4$ anode are estimated to be 1.1 J mAh^{-1} compared to that of 1.24 J mAh^{-1} in lithium metal and PEO electrolyte (1:1 weight ratio). In practice, in the case of a lithium metal anode, an excess amount of lithium metal, at least four times compared to the cathode capacity, should be used because of the dendrite formation on the anode. Therefore, the reaction heat could be estimated to reach 4.96 J mAh^{-1} or higher.

Fig.10 further shows the typical charge and discharge profiles of the full cells based on the $LiNi_{0.8}Co_{0.2}O_2$ cathode and the different anodes of lithium metal, SnSb-$Li_{2.6}Co_{0.4}N$ and $Li_{2.6}Co_{0.2}Cu_{0.2}N$-$Co_3O_4$, respectively, while operating with the PEO electrolytes at 65 ℃. The $LiNi_{0.8}Co_{0.2}O_2$/Li cell demonstrates a high working potential of 3.5-4.0 V with a capacity of 120 mAh g^{-1}, as shown in Fig.10a. Replacing the lithium metal with the insertion anodes could result into a loss in the working potential but an improvement in the safety. In general, for full utilization of lithium storage capacity of the composite anodes, the weight of cathodes has to be much over that of anodes at about 4~5 times. As can be seen from Fig.10b, the high similarity in the potential-capacity trends for the $LiNi_{0.8}Co_{0.2}O_2$/$Li_{2.6}Co_{0.2}Cu_{0.2}N$-$Co_3O_4$ cell indicates that the amorphous lithium metal nitrides remain high

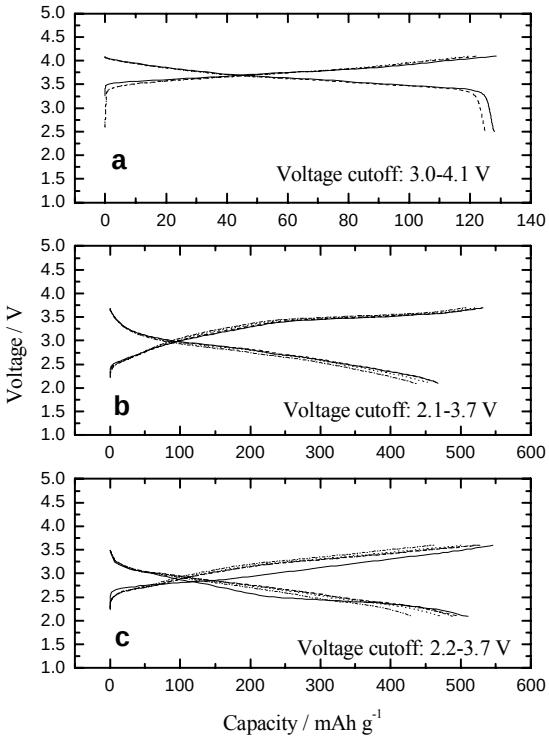

Fig.10. Charge and discharge profiles of the full cells based on $LiNi_{0.8}Co_{0.2}O_2$ cathode and anode of a) Li, b) Co_3O_4-$Li_{2.6}Co_{0.2}Cu_{0.2}N$ and c) SnSb-$Li_{2.6}Co_{0.4}N$. Electrode compositions of b) and c) are the same as in Fig.9.

stability from cycle to cycle. On the other hand, the voltage plateau of the $LiNi_{0.8}Co_{0.2}O_2$/SnSb-$Li_{2.6}Co_{0.4}N$ cell slightly increases from the first to the following cycles, which probably is attributed to the two-phase transformation of $Li_{2.6}Co_{0.4}N$ between the crystal and the amorphous, as shown in Fig.10c. The high initial coulombic efficiency of over 95 % and the large reversible anode capacity above 450 mAh g^{-1} are very remarkable for both the composite anodes, which might be highly favorable for realizing a rather high energy density and can be considered as an ideal power source for HEV & EV. However, bearing in mind that the morphological instability from the Li-alloy host is still questionable, continuous research would be pursued to develop the lithium metal nitrides-Co_3O_4 based composite electrodes proposed with low volume effects.

3.1.2 Modified graphitic carbon as insertion anodes.

From the application point of view, the first approach for lithium metal-free anode is to use graphite, as is accomplished in lithium-ion batteries with organic solvent electrolytes. The charge and discharge profile of mesocarbon microbead (MCMB, morphology as shown in Fig.11), a typical graphitic carbon used in the current lithium-ion cells, is shown in Fig.12. The very low charge efficiency of 29.7 % in the first cycle indicates that side reactions occur both in the reduction and oxidation processes which lead to some uncertainty in the determination of the maximum reversible capacity of the graphitic carbon. Consequently, its reversible capacity is

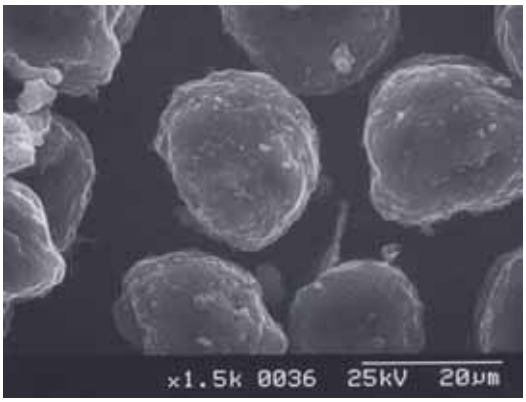

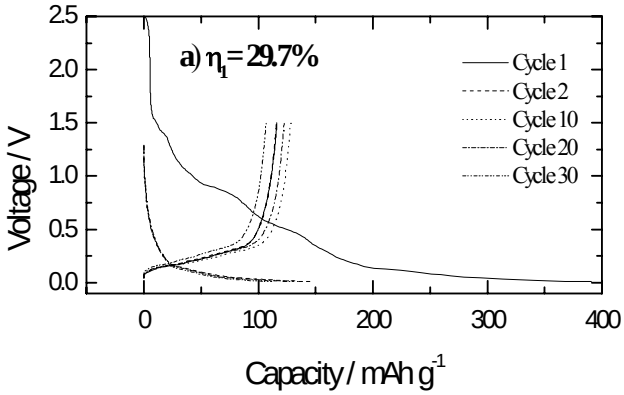

(Left) Fig.11 SEM images of the MCMB particles.
(Right) Fig.12. Charge and discharge profiles of the MCMB electrode with PEO electrolytes at 70 ℃

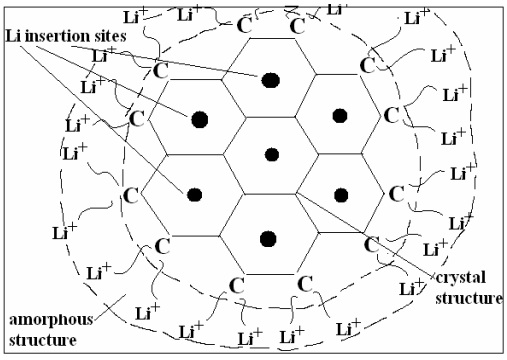

below to 150 mAh g^{-1} and the charge and discharge efficiency in the first several cycles is extremely low. Poor solid/solid interface of the graphite with the PEO electrolytes indicates that structural and interfacial performance has to be improved.

To make the graphitic carbon operate well with PEO electrolytes, we design an ionic conducting LiC_x layers by directly reacting the opened C-atom with lithium under special conditions (such as high pressure and low temperature) on the surface of the graphitic carbon that can prevent the side reaction

Fig.13. Structural images of the modified graphitic carbon.

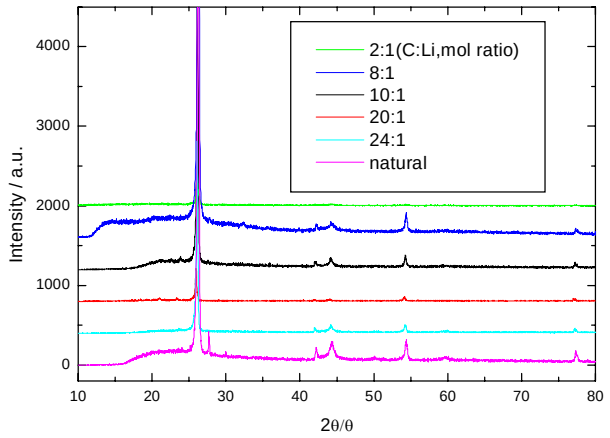

Fig.14 XRD of the modified MCMB under different Li/C ratio.

in the interface between the electrode and the PEO electrolyte, as shown in Fig.13. Due to high Li-reactivity of its surface, MCMB is chosen and treated by high energy ballmilling with lithium metal by the aid of dodecane ($\{CH_3(CH_2)_{10}CH_3\}$) under Ar. The high energy balmilling can make the surface of MCMB become disordered and therefore surface C-atom become open and further can react with Li.

Fig.14 shows that the typical crystalline structure of the treated MCMB remains to be unchanged which can permit lithium reversible insertion and extraction. XPS results as shown in Table 1 confirmed the formed LiC_x layer on the graphite surface. TEM observation shown in Fig.15 further reveals that the MCMB loss crystal on its surface upon treatment, indicating that the formed LiC_x is prevailed by amorphous or micro-crystalline phase. Cyclic voltammogram measurement as shown in Fig.16 indicates that the side

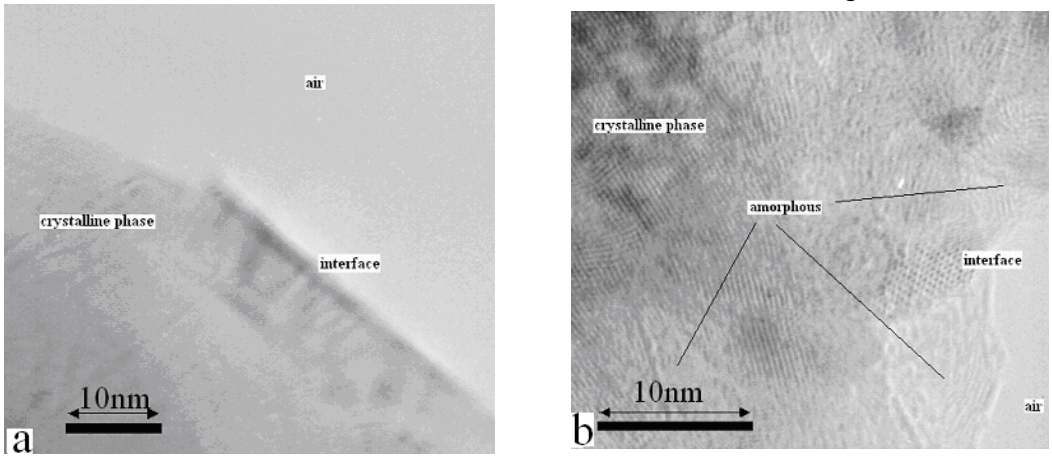

Fig.15. TEM images on the surface of the MCMB at left) without modification and right) after modification.

irreversible reaction in the first cycle is highly suppressed after the treatment, which is favorable for the electrochemical kinetics during lithium insertion into and extraction from the layered carbon. Finally, Fig.17 shows that the modified MCMB with PEO electrolytes presents an attractive behavior similar to that based on the common liquid electrolytes. Li intercalation into the graphitic hosts possesses several stages below to 200 mV. However, in the real battery testing, only one potential plateau between 0.2-0 V can be distinguished, which is correspond to the LiC_x compound reaction in an equilibrium phase. The capacity as a function upon the cycles also demonstrates high stability, as shown in Fig.18. The reversible capacity is measured to be about 290 mAh g^{-1}, which is very comparable and close to the theory data (LiC_6). Furthermore, we compared the thermal stability of the MCMB with metallic lithium while operating with the PEO electrolytes via DSC measurement, as shown in Fig.19. MCMB shows very low reaction heat under high Li utilization with the PEO electrolytes in comparison with lithium metal anode. Such a thermal behavior is highly opposite to the one based on liquid electrolytes, in which the heat generation of graphite is very significant, especially, that of the reaction heat of PVDF and LiC_x [11]. This result indicates that graphitic carbon might be a suitable anode candidate in large size rechargeable lithium-ion batteries based on PEO electrolytes for EV in terms of structural stability and thermal reliance stability.

Table.1. XPS results of the MCMB with and without treatment.

		Li_{1s}	**C_{1s}**	**F_{1s}**	**O_{1s}**
Without treatment	Binding energy	0	285 ev,	0	533.00 ev,
	Chemical composition	0	97.81%	0	2.19%
With treatment	Binding energy	56.10 ev,	291 ev,	0	532.80 ev
	Chemical composition	2.23 %	37.50 %	0	60.20 %

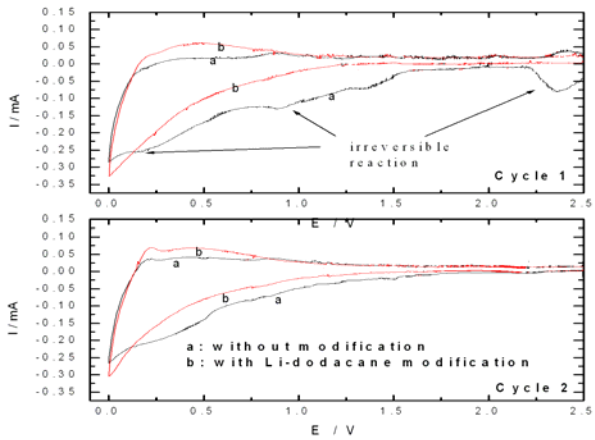

Fig.16. Cyclic voltammogram of the electrode based on a) no modified MCMB, b) $Li_{2.6}Co_{0.2}Cu_{0.2}N$ and c) Co_3O_4-$Li_{2.6}Co_{0.2}Cu_{0.2}N$ at the scan rate of 0.05 mV S^{-1}, voltage cutoff: 1.4-0. V, vs. Li/Li^+.

3.2 Cathode

The selection for proper cathodes is according to the following requirements, such as inexpensive, environmentally benign, wide operating temperature, good capacity/cycling performance, extremely safe. Transition metal oxides, such as $LiCoO_2$, layered $LiNiO_2$ and $LiMn_2O_4$ have found application as positive electrode materials for high power applications. These materials provide high potentials (about 4 V vs. Li) and good reversible capacities (about 120 mA h g^{-1}). The use of $LiMn_2O_4$ solves problems related to cost and Co and Ni toxicity, but the disproportionation of Mn^{3+} remains a severe problem. Pervious research reveals that most of the current cathodes suffers from side reaction with PEO electrolytes and detrimental phase transitions above 70 ℃ that inevitably cause to capacity loss and fade while being oxidized at a high potential. In this work, in comparison with several cathode materials, such as Li_xCoO_2 ($0.5<x<1$, 0.5-electron reaction, Cap=137 mAh g^{-1}), $Li_xMn_2O_4$ ($0<x<1$,

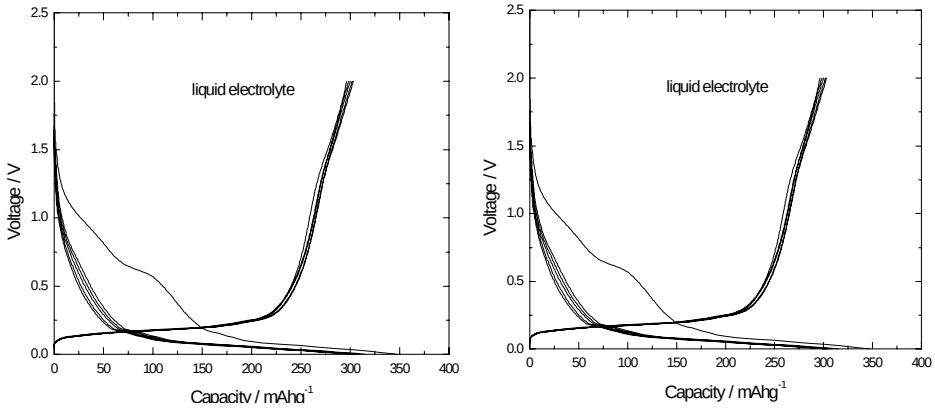

Fig.17. Comparison in the charge and discharge profiles of the MCMB based on liquid electrolytes and the modified MCMB based on PEO electrolytes.

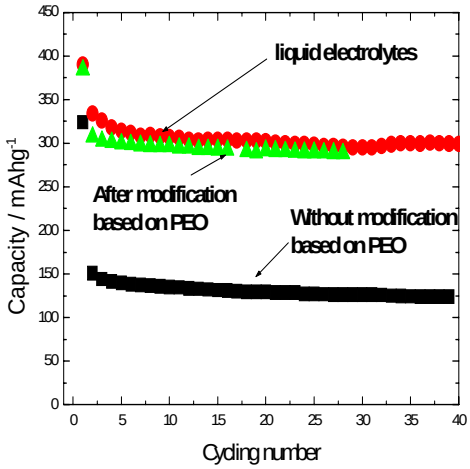

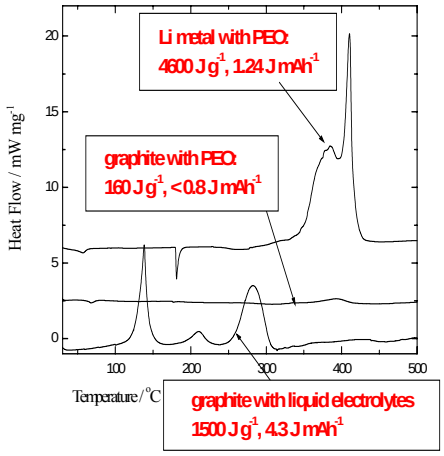

(Left) Fig.18. Cycling performance of different MCMB electrodes with liquid and PEO electrolytes.

(Right) Fig.19. DSC curves of different electrode with PEO and liquid electrolytes.

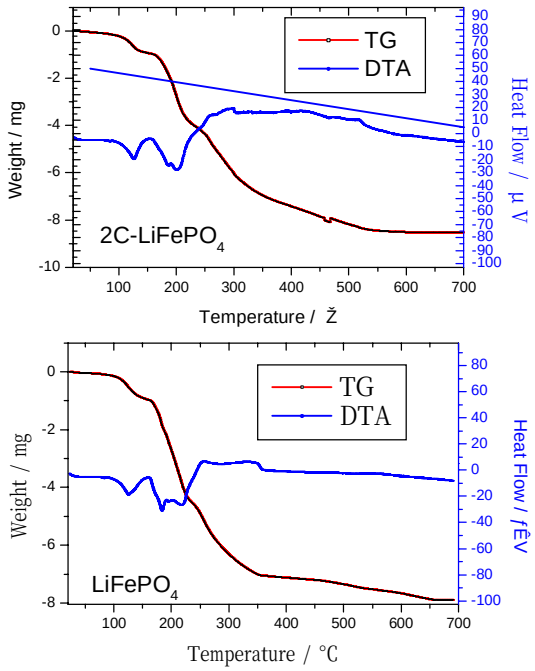

Fig.20. TG/DTA curves of the $LiFePO_4$ with and without PVC during heating to 700 ℃.

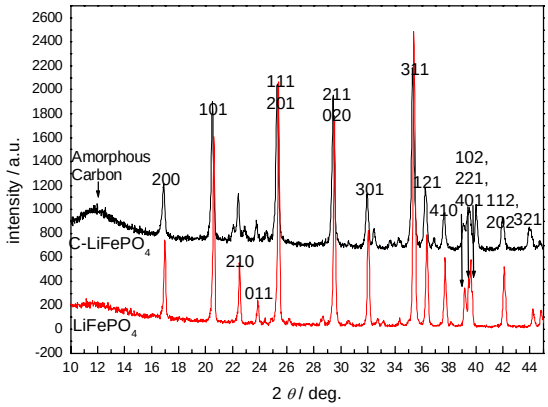

Fig.21. XRD of the resulting $LiFePO_4$ and $LiFePO_4$/C powders.

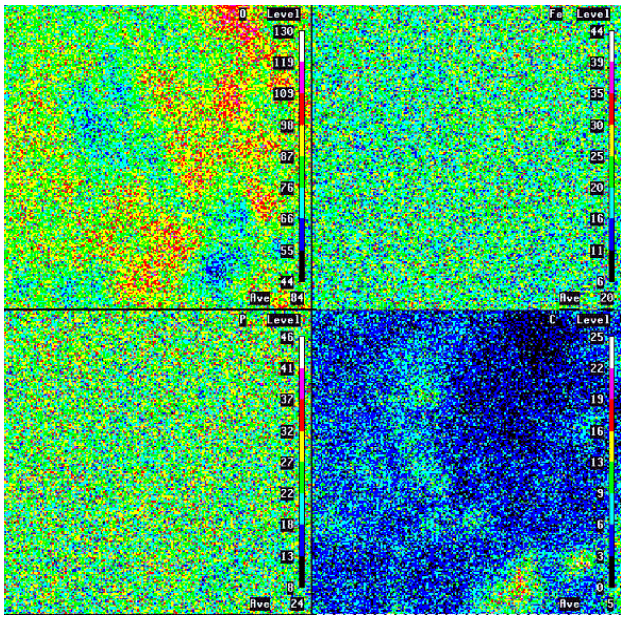

Fig.22. EPMA images of elemental distribution of the resulting materials.

Fig.23. SEM images of the resulting $LiFePO_4$/C powders.

0.5-electron reaction, Cap=148 mAh g^{-1}) and Li_xFePO_4 ($0<x<1$, 1-electron reaction, Cap=170 mAh g^{-1}), olivine type $LiFePO_4$ is very attractive due to its capability to operate within a very flat voltage plateau (around 3.5 V), high thermal stability, high working temperature performance similar to PEO electrolytes, low lattice volume changes, low cost and benign environmental properties [12].

However, a significant drawback of the $LiFePO_4$ is its poor rate capability caused by poor electron conductivity. In this work, we use poly (vinyl chloride) as carbon sources to produce the $LiFePO_4$/C composite by means of two pyrolysis reactions. The electronic conductivity of the $LiFePO_4$ can be substantially enhanced by dispersing fine particle size of the active hosts in the carbon matrix. With this modification, the $LiFePO_4$ is capable of providing high capacity and high charge rates. TG/DTA analysis conducted on the product upon the heating process shown in Fig.20 reveals that the $LiFePO_4$ possesses several decomposition reaction related to the starting materials. The PVC does not cause to a reaction with the $LiFePO_4$. The carbon contents of the $LiFePO_4$/C was confirmed to be about 5-7.5 wt% with the TG analysis. XRD technique confirms the crystalline structure of the composite proposed, as shown in Fig.21. As well, pyrolyzed carbon that is prevailed with disordered structure can be found in the product. Carbon coating process does not bring a obvious change in the lattice parameters of the $LiFePO_4$, as shown in table.2, indicating the thermal pyrolysis mainly causes to a modification in the morphology. The homogeneous distribution of the active hosts within the carbonaceous matrix is further evidenced by the elemental distribution

mapping from Electron Probe Micro-Analysis (EPMA) shown in Fig.22. SEM observation shown in Fig.23 further reveals that the material possesses high porosity which is favorable for increasing the reactive area and therefore the electrochemical kinetics. It suggests that the introduction of highly dispersed PVC has an effect on preventing the single $LiFePO_4$ growth during heating process. Meanwhile, the possible aggregation of the active hosts during high temperature could be highly barred, resulting in fine grains of the active hosts which favorable for the electrochemical kinetics. Finally, Fig.24 and 25 show that the $LiFePO_4$/C electrode presents a stable working potential at about 3.5 V vs .Li/Li^+ and a capacity of 120 mAh g^{-1}, as well as excellent cycling stability, probably due to the low lattice volume changes with Li insertion/extraction and good interfacial compatibility with the solid PEO electrolytes. The primary results suggest that the modified olivine type $LiFePO_4$ might be a good cathode candidate for the PEO electrolytes.

Table.2. Lattice parameters of the resulting compounds.

	a-axis	b-axis	c-axis	Cell volume	Crystal structure
$LiFePO_4$	10.380	6.023	4.714	294.777	Orthorhombic
2C-$LiFePO_4$	10.381	6.015	4.711	294.203	Orthorhombic

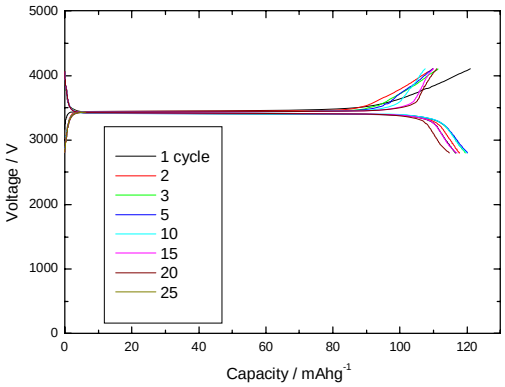

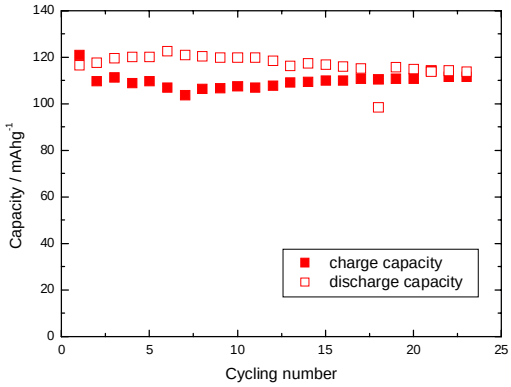

(Left)Fig.24. Typical charge and discharge profiles of $LiFePO_4$/C with PEO electrolytes at 65 ^oC (2.8-4.1 V).
(Right) Fig.25. Cycling performance of the $LiFePO_4$/C with PEO electrolytes at 65 ^oC.

4. Conclusions

1) Composite anodes based on hexagonal lithium metal nitrides have been developed to show larger capacity and higher first cycle efficiency over the current graphitic anodes. However, the performance of the composite anodes containing Li-alloy hosts is still in doubt due to that the Li-alloy has a morphological instability along with an increased heating generation dependent on Li-insertion. In contrast, the composite anodes containing lithium transition-metal nitrides and Co_3O_4 demonstrate high first charge efficiency of 100 % and large capacity of 500 mAh g^{-1}, as well as high cycling stability and low reaction heating under high Li-utilization with the PEO electrolytes, indicating that they possess potential applications in large size rechargeable lithium-ion batteries for EV in terms of high first-cycle charge efficiency, large capacity and high thermal reliance;

2) Graphitic carbon that is currently used in commercial Li-ion batteries can be successfully operated with the PEO electrolytes by designing an amorphous LiC_x layer on its surface which can prevent the side reaction. The material treating process is effective and comparable in production. The modified graphitic carbon demonstrates good electrochemical behavior similar to that in liquid electrolytes. Furthermore, high thermal stability of the graphitic carbon with PEO electrolytes under deep Li utilization suggests that the graphitic carbon might be suitable anode candidates in large size rechargeable lithium-ion batteries for EV based on PEO electrolytes in terms of structural stability and thermal reliance;

3) $LiFePO_4$/C composite has been prepared by two pyrolysis processes using poly (vinyl chloride) as carbon sources. The material was confirmed to be of high porosity and homogeneous distribution of active hosts within the carbonaceous matrix. Primarily electrochemical results indicate that the olivine type $LiFePO_4$/C is a promising cathode candidate in terms of stable working potential, acceptable capacity, high charge/discharge efficiency and excellent cycle life with the PEO electrolytes at the elevated temperature.

References

[1] Y.Aihara, M.Kodama, K.Nakahara, H.Okise, K. Murata, J. Power Sources 65, 143 (1997).
[2] M.D. Farrington. J. Power Sources 96, 260 (2001).
[3] D. Fauteux and R. Koksbang, J. Appl. Electrochem. 23, 1 (1993)
[4] J. O. Besenhard, J. Yang and M. Winter, J. Power Sources 68, 87 (1997)
[5] M. Nishijima, T. Kagohashi, N. Imanishi, Y. Takeda, O. Yamamoto and S. Kondo, Solid State Ionics, 83, 107 (1996).
[6] M. Nishijima, T. Kagohashi, N. Imanishi, Y. Takeda, O. Yamamoto, J. Power Sources, 68, 510 (1996).
[7] Y. Liu, K. Horikawa, M. Fujiyosi, N. Imanishi, A. Hirano and Y. Takeda, J. Electrochem. Soc., 151, A1450 (2004).
[8] Y. Liu, T. Matsumura, N. Imanishi, T. Ichikawa, A. Hirano, Y. Takeda, Electrochemistry Communications, 6, 632 (2004).
[9] P. Poizot, S. Laruelle, S. Grugeon, L. Dupont, J-M. Tarascon, Nature, 407, 496 (2000).
[10] J. Yang, Y. Takeda, N. Imanishi and O. Yamamoto, J. Electrochem. Soc., 147, 1671 (2000)
[11] Ph. Biensan, B. Simon, J.P. Peres, A.de. Guiber, M. Broussely, J.M. Bodet and F. Perton, J. Power Sources, 81-82, 906 (1999).
[12] A.K. Padhi, K.S. Nanjundaswamy, J.B. Goodenough, J. Electrochem. Soc. 144 (1997) 1188

Department of Electrical and Electronic Engineering

*nonmember

A Study about the Posture and Joint Stiffness at Stationary Force Control of Human Arm, Syugo UCHIDA, Satoshi KOMADA, and Junji HIRAI: Proceedings of the 8th International Workshop on Advanced Motion Control, pp.359-362, 2004.

The purpose of our research is to realize a simple and high performance control of robots using strategy of human arm operation. This time, we measure joint angle and joint stiffness of human arm during force control. When tip force is large, human being selects the posture using joint torque minimum index. When tip force is small, human being selects the posture so that manipulability becomes large. Moreover, the wrist stiffness becomes large so as to keep the posture. In order to adapt for perturbation, a regulator to avoid joint torque saturation is introduced. The effectiveness of this strategy is confirmed by a simulation result of human arm.

Joint Design Method Based on Coprime Factorization of 2DOF Control System, Tsuyoshi HIOKI, Kazuhiro YUBAI, and Junji HIRAI: Proceedings of the 8th International Workshop on Advanced Motion Control, pp.523-527, 2004.

In many cases, control system synthesis is formulated as minimization of prescribed closed loop performance reflecting control requirements. Since the closed loop performance is a function of a controlled plant and a controller, a model identification and a controller design must interact with each other. This motivates us to consider the model identification and the controller design simultaneously. However, most of the previous joint design methods are not applicable to unstable plants because the identified plant model is usually used as the design parameter. On the other hand, we have analyzed the internal structure of 2DOF control system using a coprime factorization on RH_∞ and shown that two free parameters, K and Q RH_∞, specify the tracking performance and the feedback performance, respectively. Also Tay et.al have proposed a parameterization of the plant dynamics by switching the role of the controlled plant and the controller, and introduced a free parameter R belonging to RH_∞. In this paper, we propose a new joint design strategy based on the identification of R and the design of Q. Since the identified plant parameter R is always stable, the proposed joint design strategy can be applied to a wider class than the conventional joint design method.

Fault-Tolerant Control System of Flexible Arm for Sensor Fault by Using Reaction Force Observer, Yu IZUMIKAWA, Kazuhiro YUBAI, Junji HIRAI: Proceedings of the 8th International Workshop on Advanced Motion Control, pp.583-588, 2004.

In recent years, control system reliability has received much attention with increase of situations where computer-controlled systems such as robot control systems are used. In order to improve reliability, control systems need to have abilities to detect a fault (fault detection) and to maintain stability and control performance (fault tolerance). In this paper, we address the vibration suppression control of a one-link flexible arm robot. Vibration suppression is realized by an additional feedback of a strain gauge sensor attached to the arm besides motor position. However, a sensor fault (e.g., disconnection) may degrade the control performance and make the control system unstable at its worst. In this paper, we propose a fault tolerant control system for strain gauge sensor fault. The proposed control system has a strain gauge sensor signal observer based on the reaction force observer and detects the fault by monitoring the estimation error. After fault detection, the proposed control system exchanges the faulty sensor signal for the estimated one and switches to a fault mode controller so as to maintain the stability and the control performance. We

apply the proposed control system to the vibration suppression control system of a one-link flexible arm robot and confirm the effectiveness of the proposed control system by some experiments.

Tracking of Moving Object by Manipulator Using Estimated Image Feature and Its Error Correction on Image Planes, Dai NISHIO, Masaru NAKAMURA, Satoshi KOMADA, and Junji HIRAI: Proceedings of the 8th International Workshop on Advanced Motion Control, pp.653-657, 2004.

This paper proposes a new visual servo system compensating delay time of image processing. To obtain an image feature without delay time, variation of image feature of manipulators during delay time is estimated by a Jacobian matrix from joint velocity to image feature. An image feature of moving object during delay time is estimated from a simple model by using the average velocity/acceleration that are calculated from the past image data. Moreover, its estimation error is reduced by a method based on past estimation error. The effectiveness of the proposed strategy is confirmed by a tracking of a moving object by a manipulator.

A Preliminary Study for Reconfigurable Robot System, Akihiko MATSUURA, Yuji ISHIKURA, and Junji HIRAI: Proceedings of the 30th Annual Conference of the IEEE Industrial Electronics Society (IECON 2004), vol. 2, pp.1052-1057, 2004.

In order to expand the scope of robot application, the robot should cope with the divergence of the assigned tasks and surrounding environments. With the conventional type of robot, however, the scope of the application is limited due to the lack of its reconfigurability. The authors, therefore, propose to realize a novel robot called reconfigurable robot, which is capable of changing its structure adaptively to the situation and the given tasks. The fundamental features of the robot are introduced and problems to be solved for its realization are described in this paper.

Preliminary Study on Robotic Exercise Therapy, Takashi HISADA, Noboru OKUYAMA, Satoshi KOMADA, and Junji HIRAI: Proceedings of the 30th Annual Conference of the IEEE Industrial Electronics Society (IECON 2004), vol. 3, pp.2780-2785, 2004.

This paper proposes a new concept of robotic exercise that displays human muscle force during rehabilitation procedures. The estimation is made by combination of an isokinetic dynamometer improved from its original usage for rehabilitation and a conventional muscle force estimation method based on a musculo-skeletal model which has been applied for human gait analysis. The novel isokinetic dynamometer the authors developed has a force sensor for the musculo-skeletal model analysis, and provides an arbitrary training trajectory control function. The musculo-skeletal model analysis is constructed limitedly to the under limb movement, and the muscle force estimation is made in the thigh area by employing the two optimization methods. As a result of experiments, we confirmed that there is really not much difference between the results of two methods.

Harmonic Current Suppression Using Repetitive Control for Improvement of PMSM Control Performance, Jeong-seong KIM, Shinji DOKI, Muneaki ISHIDA : IEEJ Trans. IA, Vol. 124, No. 12, pp. 1189-1196, 2004

Flashing Phenomena in Square Wave Alternating Current –Flash Welding Control by Use of PWM Inverter Power

Supply (1st Report)-, Yukihiko SATO, Muneaki ISHIDA : Quar. J. JWS, Vol. 22, No. 3, pp. 417-423, 2004

Continuous Flashing Control Using PWM Inverter –Flash Welding Control by Use of PWM Inverter Power Supply (2nd Report)-, Yukihiko SATO, Muneaki ISHIDA : Quar. J. JWS, Vol. 22, No. 3, pp. 424-429, 2004

Resistance Heating Control with A Few Flashing Using PWM Inverter –Flash Welding Control by Use of PWM Inverter Power Supply (3rd Report)-, Yukihiko SATO, Muneaki ISHIDA : Quar. J. JWS, Vol. 22, No. 3, pp. 430-434, 2004

Basic Study on Conductive Characteristics of SiC Power Device for Its Application to AC/DC Converter, Tatsuya MATSUKAWA, Hirotaka CHIKARAISHI*, Yoshihisa SATO*, Ryuichi SHIMADA* : IEEE Trans. on Applied Superconductivity, Vol. 14, No. 2, pp. 690-692, 2004

Modeling of a Small Wind Power Generating System and Design of its Control System, Takashi NONOYAMA, *Shengtie WANG, Naoki YAMAMURA and Muneaki ISHIDA: Proceedings of international conference on Electrical Engineering 2004 (ICEE 2004), p.p.525-530, 2004

Construction of Solar Module Simulator Using Linear Amplifier, Hiroto HAYASHI, Naoki YAMAMURA and Muneaki ISHIDA: Proceedings of international conference on Electrical Engineering 2004 (ICEE 2004), p.p.542-547, 2004-7

A Study of Combined-type Active Filter using Linear Power Amplifier [In Japanese], Rieko MORIYA, Naoki YAMAMURA, Muneaki ISHIDA and Takamasa HORI: IEEJ Trans. IA, Vol.124, No.5, p.p.442-449, 2004

Direct visualization of electromagnetic micro-field by superposition of three types of electron holograms, Masaaki OKUHARA*, Akinori OHSHITA, Yohei YAMAKAWA, Koichi HATA and Kazuo IIDA : Proceedings of 8th Asia-pacific Conference on Electron Microscopy, 2004

A new electron holographic method is presented for direct visualization of electromagnetic micro-fields. In this method, three types of electron holograms obtained under the same operating condition of an electron biprism are superposed. The phase information which cannot be extracted from the modified double-exposure electron hologram can be obtained. This implies that we can get the more information by using three types of electron holograms.

Direct visualization of magnetic micro-field around a barium ferrite particle by modified double-exposure electron holography, Akinori OHSHITA, Masaaki OKUHARA*, Yohei YAMAKAWA, Koichi HATA and Kazuo IIDA : Proceedings of 13th European Microscopy Congress, 2004

Double-exposure electron holography, three-electron-wave interference method and four-electron-wave interference method were developed for direct visualization of pure phase objects such as electromagnetic micro-fields. Although the three-electron-wave and four-electron-wave interference methods are very useful, two electron biprisms are indispensable. Therefore we proposed the modified double-exposure electron holographic method using an electron biprism. In this paper, we present an experimental result of magnetic-field observation with this method.

Low molecular weight of fluid in an alloy of EPDM/SIR, Kazuo IIDA and Reuben HACKAM*, 2004 Annual Report Conference on Electrical Insulation and Dielectric Phenomena, pp.607-610, 2004

Ethylene propylene diene rubber (EPDM), silicone rubber (SIR) and their alloys have good performance when used as outdoor insulators. The hydrophobicity of the surface is maintained in wet and polluted conditions as a result of the presence of silicone fluid on the surface. This is sustained by the diffusion of low molecular weight (LMW) fluid from the bulk to the surface. The amount of LMW fluid on the surface and in the bulk of the material determines the hydrophobicity during the lifetime of the alloy of EPDM/SIR used as insulators. A study of the amount, loss and generation of the LMW fluid in an alloy of EPDM/SIR used for outdoor insulators has been performed as a function of temperature in order to simulate the effects of the heat generated by the dry band arcings on the surface. From an infrared (IR) spectroscopy study, the LMW fluid extracted from the virgin specimen is found to be composed of two kinds of fluids; one comes from the EPDM and the other comes from the SIR components of the alloy. The component of the fluid from the SIR initially decreases with sequential heating at 200 ^{o}C for 32 h in air and extraction by immersion in hexane at 44 ^{o}C for 96 h, but then the component of the fluid from EPDM finally becomes predominant.

Two Dimensional Motion Tracking of Left Ventricular Myocardium Using Ultrasonic Doppler Signal, Wataru OHYAMA, Toshikazu MURAMATSU, Tetsushi WAKABAYASHI, Fumitaka KIMURA, Shinji TSURUOKA, and Kiyotsugu SEKIOKA*: Proc. of the Sixth IASTED International Conference on Signal and Image Processing, pp.436-440 (#444-187), 2004

Automatic Tracking for Regional Myocardial Motion by Correlation Method with Connecting Multiple ROIs, Wataru OHYAMA, Masaki INAMI, Tetsushi WAKABAYASHI, Fumitaka KIMURA, Shinji TSURUOKA, and Kiyotsugu SEKIOKA*: IEEJ Transactions on Electronics, Information and Systems

Regional Tissue Estimation for Myocardium Using Phase Frequency Spectrum of Ultrasonic RF Signal, Yoshikadu YASUMOTO, Hirotake ISHII, Shinji TSURUOKA, Fumitaka KIMURA, Tetsushi WAKABAYASHI, Wataru OHYAMA, and Kiyotsugu SEKIOKA*: The tenth International Conference on Virtual Systems and Multimedia (VSMM2004) , pp.82-88, 2004

Hybrid Automatic Tracking of Regional Myocardium from Ultrasonic RF Echo Signal Using Cardiac Cycle Estimation, Akihiko KAWABATA, Shinji TSURUOKA, Wataru OHYAMA, Hiroharu KAWANAKA* and Kiyotsugu SEKIOKA*, The tenth International Conference on Virtual Systems and Multimedia (VSMM2004) , pp.307-310, 2004

Nurse Scheduling Support System Using Genetic Algorithm and its Development, Hiroharu KAWANAKA*, Tomohiro YOSHIKAWA, Shinji TSURUOKA, Tsuyoshi SHINOGI and Koji YAMAMOTO*, The tenth International Conference on Virtual Systems and Multimedia (VSMM2004), pp.526-535, 2004

An Individual Guidance System on Keywords Written by a Lecturer for e-Learning Using a Pen Capture Tool, Kazuyuki NISHIKIMI, Yuuki YADA, Shinji TSURUOKA, Tomohiro YOSHIKAWA and Tsuyoshi SHINOGI, The tenth International Conference on Virtual Systems and Multimedia (VSMM2004) , pp.1015-1022, 2004

The determination method of camera View Using Active Cameras and Whiteboard Capture Tool for Image Based e-Learning, Keiichi SHIRASAWA, Yuuki YADA, Shinji TSURUOKA, Tomohiro YOSHIKAWA and Tsuyoshi SHINOGI, The tenth International Conference on Virtual Systems and Multimedia (VSMM2004) , pp.1023-1032, 2004

Between-core Vector Overlapping for Efficient Core Testing of System-On-Chip LSI Circuits, Tsuyoshi SHINOGI, Yuki YAMADA, Terumine HAYASHI, Tomohiro YOSHIKAWA, Shinji TSURUOKA, The IEICE Transactions on Information and Systems, Vol.J87-D-I, No.6, pp.702-711, 2004

Test Vector Overlapping for Test Cost Reduction in Parallel Testing of Cores with Multiple Scan Chains, Tsuyoshi SHINOGI, Yuki YAMADA, Terumine HAYASHI, Tomohiro YOSHIKAWA, Shinji TSURUOKA, 5th Workshop on RTL and High Level Testing(WRTLT'04), pp.117-122, 2004

A Study for Wireless TCP Access with Base Station Diversity, Katsuhiro NAITO, Hiroshi. OKADA*, Takaya. YAMAZATO*, and Masaaki. KATAYAMA*: IEICE Transactions on Communications, vol. J87-B, no.4, pp.512-523, April 2004. [in Japanese]

Frequency Band and Time Slot Selection Scheme for Downlink Packet Communications in Cellular Band Division MC-CDM Systems, Kazuo MORI and Hideo KOBAYASHI: IEICE Transactions on Communications, Vol.E87-B No.5, pp.1114-1122, May 2004.

Clipping and Inter-modulation Noise Mitigation Method for OFDM Systems, Pisit BOONSRIMUANG, Pornphavit BOONSRIMUANG*, Kazuo MORI, Hideo KOBAYASHI and Tawil PAUNGMA*: Electrical Engineering/Electronics, Computer, Telecommunications and Information Technology Conference (ECTI-CON 2004), May 2004.

Dynamic Cell Configuration Scheme for Common Channel Communications in CDMA Cellular Packet Systems, Kazuo MORI and Hideo KOBAYASHI: IEEE International Conference on Communications (ICC2004), Paris, June

2004.

An Advanced CSMA Inter-Vehicle Communication System using Packet Transmission Timing Decided by the Vehicle Position, Tomotaka NAGAOSA*, Yukinari KOBAYASHI, Kazuo MORI and Hideo KOBAYASHI: IEEE Intelligent Vehicle Symposium (IV04), June 2004.

Proposal of SDM-SCOFDM System with Adaptive Modulation Method over MIMO Channels, Yuanrun TENG, Kazuo MORI and Hideo KOBAYASHI: IEICE Transactions on Communications, Vol. E87-B, No.9, pp.2757-2766, Sep.2004.

Radio Resource Assignment Scheme for Asymmetric Traffic in CSMA/Shared-TDD Cellular Packet Communications, Yukinari KOBAYASHI, Kazuo MORI and Hideo KOBAYASHI: IEEE Vehicular Technology Conference (VTC 2004-Fall), Sep. 2004.

Downlink Packet Transmission Control for Asymmetric Traffic in CDMA/Shared-TDD Cellular Communication Systems, Kazuo MORI and Hideo KOBAYASHI: IEEE International Symposium on Spread Spectrum Techniques and Applications (ISSSTA04), Sep. 2004.

Proposal of OFDM Channel Estimation Method using Discrete Cosine Transform, Hideo KOBAYASHI and Kazuo MORI: IEEE International Symposium on Personal, Indoor and Mobile Radio Communications (PIMRC2004), Sep. 2004.

Performance of DCT Interpolation-based Channel Estimation Method for MIMO-OFDM Systems, Yuanrun TENG, Kazuo MORI and Hideo KOBAYASHI: International Symposium on Communications and Information Technologies 2004 (ISCIT 2004), Oct. 2004.

Soft Handoff Technique for Downlink IP Packet Transmissions in Cellular Environments, Abubaker KHUMSI, Kazuo MORI and Hideo KOBAYASHI: International Symposium on Communications and Information Technologies 2004 (ISCIT 2004), Oct. 2004.

QAM-OFDM System with IDAR Method in Satellite Channel, Pist BOONSRIMUANG, Kazuo MORI, Tawil PAUNGMA and Hideo KOBAYASHI: IEICE Joint Conference on Satellite Communications 2004 (JCSAT2004), Oct. 2004.

A Study on the Simple Penalty Term to the Error Function from the Viewpoint of Fault Tolerant Training, Haruhiko TAKASE, Hidehiko KITA and Terumine HAYASHI: Proc. of 2004 International Joint Conference on Neural

Networks (IJCNN2004), pp.1045-1050, 2004

On Generating Test Data with High Compressibility, Naohhiro HIRAIWA, Terumine HAYASHI, Tsuyoshi SHINOGI, Haruhiko TAKASE, and Hidehiko KITA: Proc. of IEEE 5th Workshop on RTL and High Level Testing (WRTLT'04), pp.59-64, 2004

A CAI System for Increasing Learners' Confidence in Answers, Shinobu TABATA, Hidehiko KITA, Haruhiko TAKASE, Terumine HAYASHI and Tsutomu SHIMOMURA: Proc. of International Conference on Computers in Education 2004 (ICCE2004), CD-ROM, 2004

A System for Determining Students' Comprehension during Lectures, Naoki MORITA*, Hidehiko KITA and Kanji AKAHORI*: International Conference on Computers in Education 2004 (ICCE2004), CD-ROM, Nov. 2004

A Practical Method of Multiple-Choice Questions in Formative Tests [In Japanese], Shinobu Tabata, Naoki MORITA*, Hidehiko KITA, Haruhiko TAKASE, Terumine HAYASHI and Tsutomu SHIMOMURA: Council for Improvement of Education through Computers, Computer & education, Vol.17, pp.126-132, 2004

Influence of etching condition on surface morphology of AlN and GaN layers, Noriyuki KUWANO*, R. TAJIMA*, Shinya BOHYAMA, Hideto MIYAKE, Kazumasa HIRAMATSU and Tomohiko SHIBATA*: Phys. Stat. Sol. (a) 201, pp. 2755-2759, 2004

Time-resolved nonlinear luminescence of excitonic transistors in GaN, Yoichi YAMADA*, Yohei YOSHIDA*, Tsunemasa TAGUCHI*, Hideto MIYAKE, Kazumasa HIRAMATSU, Yasushi IYECHIKA and Takayoshi MAEDA*: J. Appl. Phys. 96, pp. 138-143 2004

Characterization of III-nitride based Schottky UV detectors with wide detectable wavelength range (360-10 nm) using Synchrotron Radiation, Atsushi MOTOGAITO, Kazumasa HIRAMATSU, Yasuhiro SHIBATA, Hironobu WATANABE, Hideto MIYAKE, Kazutoshi FUKUI*, Youichiro OHUCHI*, Kazuyuki TADATOMO* and Yutaka HAMAMURA: Mat. Res. Soc. Symp. Proc. 798, pp. 53-58 2004

Low-dislocation density GaN and AlGaN using epitaxial-lateral-overgrowth methods, Kazumasa HIRAMATSU and Hideto MIYAKE: Electrochemical Society Proceedings 2004-06, pp.472-483, 2004

Characterization of freestanding metal optical filters and GaN UV detectors in VUV and SX region, Atsushi MOTOGAITO, Hironobu WATANABE, Kazumasa HIRAMATSU*, Kazutoshi FUKUI*, Yutaka HAMAMURA* and Kazuyuki TADATOMO*: UVSOR ACTIVITY REPORT 2003, p.60, 2004

Characterization of UV detectors with n-AlGaN on AlN epitaxial films, Kazumasa HIRAMATSU, Yasuhiro SHIBATA, Hiroyuki YASUKAWA, Atsushi MOTOGAITO, Hideto MIYAKE, Youichro OHUCHI*, Kazuyuki TADATOMO*, Tatsushi NOMURA*, Yutaka HAMAMURA* and Kazutoshi FUKUI*: UVSOR ACTIVITYREPORT 2003, p. 70, 2004

Electrical and Magnetic Properties of La(Ba)MnO3 Thin Films, Tamio ENDO, Shin-ichi IWASAKI, Kouji YOSHII, Takahisa SAKURADA, Michi OGATA, Ajay SARKAR, Josep NOGUES*, Juan MUNOZ*, Jose COLINO*: Trans. Mat. Res. Soc. Jpn. 29(4), pp.1431-1436, 2004

Fabrication of YBCO and LBMO Thin Films, and Double Layered Nanocomposite, Tamio ENDO, Masanori OKADA, Michi OGATA, Takahisa SAKURADA, Ajay SARKAR: Proc. ICCE-11 (South Carilina, 2004), pp.157-158, 2004

Synthesis by MOCVD of c-axis Bi2Sr2Ca2Cu3O10 Superconducting Thin Films on (001) and (110) MgO Substrates, Kazuhiro ENDO*, Peter BADICA*, Tamio ENDO: Proc. APMC (New Delhi, 2004), pp.790-793, 2004

Microwave Absorption Depending on Field Sweep Rate and Anisotropic Vortex Dynamics in a-Oriented Superconducting YBCO Thin Film, Tamio ENDO, Akinori HASHIZUME, Masanori OKADA, Takahisa SAKURADA, Ajay SARKAR, Masashi MUKAIDA*: Proc. APMC (New Delhi, 2004), pp.698-701, 2004

Brightness of electron beam emitted from a single pentagon on a multiwall carbon nanotube tip, Koichi HATA, Akihiro TAKAKURA, Akinori OHSHITA, and Yahachi SAITO*: Surface and Interface Ana2004lysis 36, pp.506-509, 2004

A capped multiwall carbon nanotube (MWNT) with clean surface gives field emission patterns consisting of six pentagonal rings corresponding to pentagons located at the tip. To evaluate optical properties of a single pentagon as an electron source, I-V characteristics and angular current densities for a single clean pentagon have been measured by probe-hole type field emission microscopy (FEM). A reduced brightness estimated from the angular current density and the geometrical size of pentagon, reached about 5.6×10^9 A/(m^2srV) at an emission current of 53 nA. This value of reduced brightness is one order of magnitude or more higher than that of individual MWNT field emitter reported by Jonge *et al*.

Interference fringes observed in electron emission patterns of a multiwall carbon nanotube, Koichi HATA, Akihiro TAKAKURA, Kenji MIURA, Akinori OHSHITA, and Yahachi SAITO*: Journal of Vacuum Science & Technology B, 22, 3, pp.1312-1314, June ,2004

A capped multiwall carbon nanotube (MWNT) with clean surface gives field emission patterns consisting of six pentagonal rings which correspond to pentagons located at the tip end. One or a few bright streaks are also observed at the boundaries of neighboring pentagons. The spacing of streaks is inversely proportional to the square root of the accelerating voltage. Namely, the spacing changes with the wave length of emitted

electrons according to Young's interference equation. The visibility of streaks increased with the accelerating voltage, which can be explained successfully in terms of a concept of a virtual source size. These experimental results suggest that the streaks are no more than Young's interference fringes for which the adjacent pentagons behave as double slits.

Fabrication of carbon nanotube array and its field emission property, H. SATO, H. TAKEGAWA, H. YAMAJI, H. MIYAKE, K. HIRAMATSU and Y. SAITO*: Journal of Vacuum Science & Technology B 22 (3) pp.1335-1337, 2004

A novel fabrication process for carbon nanotubes (CNTs) field emitter array is reported. This process consists of formation of a protrusion on a silicon substrate, selective deposition of catalyst film on tips of the protrusions and direct growth of carbon nanotubes on the tips of the protrusions by plasma-enhanced chemical vapor deposition (PECVD). In this process, number of the CNTs grown on each tip of the protrusion can be controlled by size of the protrusion. The CNTs field emitter arrays gave better field emission property than a continuous CNTs film. A threshold voltage required to obtain $1\mu A/cm^2$ of field emission current from the CNTs field emitter array was about 300V lower than that from the continuous CNTs film. This improvement is presumably due to reduction of screening effect, which prevents the field from concentrating on the tip of the CNT emitters.

Composite Materials and Their Applications, Shuhei NAKAMURA, Yusuke AOKI, Takuya SHINDOU*, Tetsushi OKAMOTO*: Proceedings of the XXVIII International Conference of International Microelectronics & Packaging Society -Poland Chapter-(2004-9), pp. 69-76, 2004

Electrical Properties of Composite Materials and their Functionalization, Tetsushi OAKAMOTO*, Takuya SHINDOU*, Shuhei NAKAMURA: Proceedings of the 11th Annual International Conference on Composites/Nano Engineering, pp. 527-530, 2004

Functionalization of Organic-Inorganic Hybrid Materials [in Japanese]. Takuya SHINDOH*, Makoto SUGIURA, Yusuke AOKI, Shuhei NAKAMURA, Kanichi KAMIYA: Proceedings of the 35th symposium on electrical and electronic insulating materials and application in systems, pp. 97-100, 2004

Super Low-resistive Composites Made with Thermoplastic Elastomer, Graphite and Carbon Black [in Japanese], Hirotomo MINAMIYAMA, Mitsuhiro HISHIDA, Kouichi TACHI, Yusuke AOKI, Shuhei NAKAMURA: Proceedings of the 35th symposium on electrical and electronic insulating materials and application in systems, pp. 205-208, 2004

Department of Chemistry for Materials

* nonmember

Effect of "Topotactic" Reduction Product of Tungsten Disulfide on Catalytic Activity of Metallocene Catalyst for Olefin Polymerization, Satoru YAMADA, Akihiro YANO*, Morihiko SATO*, Takahito ITOH : Journal of Molecular Catalysis A: Chemical 208, pp. 55-65, 2004

N,N-Dimethylanilinium ($Ph(Me)_2NH^+$) salt of tungsten disulfide (WS_2) was developed as a novel cocatalyst for metallocene catalysts. The cocatalyst is composed of *N,N*-dimethylanilinium ion as a cationic part and "topotactic" reduction product of WS_2, obtained by acquisition of an electron by the neutral host lattice of WS_2 without structural alteration, as an anionic part. Notable improvement of the catalytic activity for ethylene polymerization using the bis(indenyl)zirconium dichloride (Ind_2ZrCl_2)/triethylaluminum (Et_3Al) catalyst was observed upon the addition of the $Ph(Me)_2NH^+$ salt of WS_2. The addition of the corresponding molybdenum disulfide (MoS_2) one that had smaller crystallite size than the $Ph(Me)_2NH^+$ salt of WS_2 showed the lower catalytic activity. The resultant poly(ethylene) prepared by the $Ind_2ZrCl_2/Et_3Al/Ph(Me)_2NH^+$ salt of WS_2 possessed similar properties like narrow polydispersity to that prepared by conventional metallocene type catalysts. The Zr loadings on the precipitate of the Ind_2ZrCl_2/Et_3Al catalyst activated by the $Ph(Me)_2NH^+$ salt of WS_2 increased with a decrease in the crystallite size of the $Ph(Me)_2NH^+$ salt of WS_2. However, the catalytic activities in ethylene polymerization decreased drastically, indicating that the decrease of the crystallite size led to the significant increase of inactive species for ethylene polymerization.

Spontaneous Polymerization Mechanism of 7,7-Dicyanobenzoquinone Methide with p-Methoxystyrene, Yukihiro MITSUDA, Shuji KAWAGUCHI, Takahiro UNO, Masataka KUBO, Takahito ITOH : Macromolecules 37, pp. 1251-1256, 2004

Spontaneous polymerization of 7,7-dicyanobenzoquinone methide (CQM) with p-methoxystyrene (MeOSt) was investigated. An alternating copolymer of CQM with MeOSt was obtained as the hexane-insoluble product, and a small amount of a 1:2 cycloadduct of CQM:MeOSt in addition to large amounts of unreacted CQM and MeOSt was obtained as the hexane-soluble product. To clarify an active intermediate in this reaction, spontaneous polymerizations of CQM with MeOSt were carried out in the presence of additives such as 2,2,6,6-tetramethylpiperidine-1-oxy (TEMPO) and acetic acid and in three solvents with different polarity. The spontaneous reaction in the presence of the TEMPO did not afford any products trapped by TEMPO. On the other hand, the reaction in the presence of acetic acid gave a 1:1:1 adduct of CQM:MeOSt:acetic acid in a quantitative yield. It was concluded from these results that the spontaneous polymerization of CQM with MeOSt might proceed via a zwitterionic intermediate, which has gauche and trans forms.

Crystal Structures and Topochemical Polymerizations of 7,7,8,8-Tetrakis(alkoxycarbonyl)quinodimethanes, Shinji NOMURA, Takahito ITOH, Hirofumi NAKASHO, Takahiro UNO, Masataka KUBO, Kazuki SODA*, Katsunari INOUE*, Mikiji MIYATA* : Journal of American Chemical Society 126, pp. 2035-2041, 2004

Highly conjugated monomers, 7,7,8,8-tetrakis(alkoxycarbonyl)quinodimethanes (methoxy (1a), ethoxy (1b), isopropoxy (1c), benzyloxy (1d), chloroethoxy (1e), and bromoethoxy (1f)), were synthesized. Recrystallizations of 1a, 1c, 1e, and 1f yielded two crystal forms (prisms (1a-A) and needles (1a-B), needles (1c-A) and plates (1c-B), prisms (1e-A) and plates (1e-B), and prisms (1f-A) and needles (1f-B)), which have different molecular packing modes by X-ray crystal structure analysis, indicating that the crystals are polymorphic. In the photopolymerizations of these monomer crystals in the solid state, 1a-A, 1e-A, and 1f-A polymerized topochemically to give crystalline polymers. For their thermal polymerizations in the solid state, in addition to 1a-A, 1e-A, and 1f-A, 1e-B and 1f-B polymerized, but polymers formed from the 1e-B and 1f-B were amorphous. The packing of quinodimethane molecules in the crystals was defined by four kinds of parameters, stacking distance (d_s), the distance between the reacting exomethylene carbon atoms (d_{cc}), the angles formed between the stacking axis and longer axis of the monomer molecule (θ_1), and the shorter axis of the monomer molecule (θ_2), and then the polymerization reactivity of these quinodimethanes in the solid state was discussed on the basis of these parameters.

Ionic Conductivity and Mechanical Property of Cross-linked Hyperbranched Polymer Electrolytes for Lithium Secondary Batteries, Takahito ITOH, Seiji HORII, Shinya HASHIMOTO, Takahiro UNO, Masataka KUBO, Osamu YAMAMOTO* : Transaction of the Materials Research Society of Japan 29, pp. 1025-1030, 2004

Composite polymer electrolytes composed of cross-linkable hyperbranched polymer (HBP), poly[bis(triethylene glycol)benzoate] capped with acetyl and/or acryloyl groups in various ratios, poly(ethylene oxide), $BaTiO_3$ as an inorganic filler, and $LiN(CF_3SO_2)_2$ as a lithium salt were prepared by solvent casting, followed by thermal cross-linking, and their ionic conductivities and mechanical properties were investigated.

Preparation of Mechanically Cross-Linked Polystyrenes, Masataka KUBO, Naoki KATO, Takahiro UNO, Takahito ITOH : Macromolecules 37, pp. 2762-2765, 2004

This paper reports preparation of mechanically cross-linked polystyrenes using cyclic macromonomer as a nonbonding cross-linking agent. Emulsion and thermal self-initiated copolymerizations of styrene with a well-defined cyclic macromonomer based on a cyclic polystyrene were carried out to obtain mechanically cross-linked polystyrenes with high swellability. Mechanically cross-linked chloromethylated polystyrene was prepared by thermal self-initiated terpolymerization of the cyclic macromonomer, styrene, and 4-vinylbenzyl chloride.

Spontaneous Polymerization Mechanism of 7,7-Dicyanobenzoquinone Methide with 1,3-Cyclohexane, Shuji KAWAGUCHI, Yukihiro MITSUDA, Takahiro UNO, Masataka KUBO, Takahito ITOH : Kobunshi Ronbunshu 61, pp. 263-268, 2004

Spontaneous polymerization of 7,7-dicyanobenzoquinone methide (CQM) with 1,3-cyclohexane (CHD) was investigated. The spontaneous reactions gave alternating copolymers of CQM with CHD, where CHD units were incorporated in 1,2- and 1,4-addition structures, as

hexane-insoluble products and a Diels-Alder adduct of CQM with CHD as hexane-soluble product. Addition of acetic acid to the spontaneous polymerization system did not affect the composition and distribution of products. On the other hand, the spontaneous polymerization in the presence of 2,2,6,6-tetramethylpiperidine-1-oxyl (TEMPO) gave a low molecular weight alternating copolymer with TEMPO at the terminal end as hexane-insoluble product and a 1:1:1 adduct as hexane-soluble product. It was concluded from these results that the spontaneous polymerization of COM with CHD proceeds via a diradical intermediate.

Influence of Hyperbranched Polymer Structure on Ionic Conductivity in Composite Polymer Electrolytes of PEO/Hyperbranched Polymer/$BaTiO_3$/Li Salt System, Takahito ITOH, Seiji HORII, Takahiro UNO, Masataka KUBO, Osamu YAMAMOTO* : Electrochimica Acta 50, pp. 271-274, 2004

The influence of the hyperbranched polymer (HBP) structure such as molecular weights, molecular weight distribution, chain-end, ethylene oxide (EO) chain lengths on the ionic conductivity of the composite polymer electrolytes composed of poly(ethylene oxide) (PEO), $BaTiO_3$ as a ceramic filler, $LiN(CF_3SO_2)_2$ as a lithium salt, and HBP as a plasticizer were investigated. The difference in the molecular weights of the HBP did not affect significantly the ionic conductivity. However, molecular weight distribution of the HBP might affect the ionic conductivity of the composite polymer electrolyte, which decreased with broadening of the molecular weight distribution. Further branching at the chain-end structure in the HBP led to a decrease in the ionic conductivity. The HBP with a longer EO chain length was effective to an enhancement of the ionic conductivity.

Spontaneous Polymerization Mechanism of Electron-Accepting Substituted Quinodimethane with Vinyl Ether and Cyclic Ketene Acetal, Yukihiro MITSUDA, Takashige FUJIKAWA, Katsumi NAKASAKA, Takahiro UNO, Masataka KUBO, Takahito ITOH, Journal of Polymer Science: Part A: Polymer Chemistry 42, pp. 3800-3811, 2004

The spontaneous reactions of 1-(2,2-dimethyl-1,3-dioxane-4,6-dione-5-ylidene)-4-(dicyano-methylene)-2,5-cyclohexadiene (QM-1) with a vinyl ether, butyl vinyl ether (BVE), and a cyclic ketene acetal, 2-methylene- 1,3-dioxepane (MDOP), were investigated. The reaction of QM-1 with BVE produced a terpolymer composed of QM-1, 7-butoxy-8,8-dicyanoquinodimethane, and BVE units as a hexane-insoluble product and a one-to-one adduct of methylene Meldrum's acid and BVE as a hexane-soluble product. The spontaneous reaction of QM-1 with BVE produced, in the presence of 2,2,6,6-tetramethylpiperidine-1-oxy (TEMPO), a terpolymer carrying TEMPO units in the chain ends, and in the presence of methanol, a one-to-one-to-one adduct of QM-1, BVE, and methanol was isolated. The spontaneous reaction with bulkier, electron-donating MDOP produced a low-molecular-weight alternating cooligomer of QM-1 with MDOP. The spontaneous polymerization was proposed to proceed via a zwitterionic intermediate taking two forms, gauche and trans, depending on the bulkiness of the comonomer.

Asymmetric Anionic Polymerization of 2,6-Dimethyl-7-phenyl-1,4-benzoquinone Methide, Takahiro UNO, Masaya MINARI, Masataka KUBO, Takahito ITOH : Journal of Polymer Science: Part A: Polymer Chemistry 42, pp. 4548-4555, 2004

Asymmetric anionic polymerizations of 2,6-dimethyl-7-phenyl-1,4-benzoquinone methide (1) were performed with various chiral anionic initiators, and the specific rotations of the obtained polymers were investigated. Optically active poly(1)s with configurational chirality were obtained with all the initiators, and a complex of fluorenyllithium (FlLi) with (-)-sparteine [(-)-Sp] produced poly(1) with the largest negative specific rotation ($[\alpha]_{435}$ = -26.8°). The specific rotations of poly(1)s obtained with FlLi/(-)-Sp depended on the initiator concentration and the solvent polarity. The maximum specific rotations were obtained at an almost constant initiator concentration (ca. 0.03 mol/L), regardless of the monomer concentration, in toluene, whereas a higher initiator concentration was required in more polar solvents. These results suggested that the aggregation state of the propagating chain end significantly affected the specific rotation of poly(1).

Solid-State Polymerization of 7-Alkoxycarbonyl-7-cyano-1,4-benzoquinone Methides, Takahito ITOH, Shinji NOMURA, Nagisa SAITOH, Takahiro UNO, Masataka KUBO, Kazuki SODA*, Katsunari INOUE*, Mikiji MIYATA* : Macromolecules 37, pp. 7938-7944, 2004

Thermal polymerizations and photopolymerizations of 7-alkoxycarbonyl-7-cyano-1,4-benzoquinone methides (methoxy (2a), ethoxy (2b), propoxy (2c), isopropoxy (2d), butoxy (2e), and sec-butoxy (2f)) were investigated in the solid state. In the thermal polymerization in the solid state, 2a, 2c, 2d, and 2e polymerized to give glassy solids or a mass of crystals, but both 2b and 2f did not polymerize. In the photopolymerization in the solid state, all monomer crystals except for 2a polymerized to give corresponding polymers as needlelike solids. The needlelike polymer obtained by photopolymerization of highly reactive 2c was amorphous by powder X-ray diffraction measurement. Crystal structure of 2c was determined by single-crystal X-ray structure analysis, and the molecular packing in the crystals was discussed.

Molecular Oxygen Insertion Polymerization into Crystals of Tetrakis(alkoxycarbonyl)quino-dimethanes, Takahito ITOH, Shinji NOMURA, Masaki OHTAKE, Takafumi YOSHIDA, Takahiro UNO, Masataka KUBO, Atsushi KAJIWARA*, Kazuki SODA*, Mikiji MIYATA* : Macromolecules 37, pp. 8230-8238, 2004

Solid-state alternating copolymerization took place by molecular oxygen insertion in the crystals of 7,7,8,8-tetrakis(ethoxycarbonyl)quinodimethane (1a) and 7,7-bis(ethoxycarbonyl)-8,8-bis(methoxycarbonyl) quinodimethane (1b) to form highly crystalline needlelike white solids for 1a and amorphous ones for 1b. The polymer structures were confirmed by ^{1}H NMR, ^{13}C NMR, IR, elemental analysis, powder XRD, and TGA measurements. However, in vacuo polymerizations of 1a and 1b in the solid state with heating and photoirradiation did not take place. 7,7,8,8-Tetrakis(methoxycarbonyl)quinodimethane (1c) did not undergo solid-state alternating copolymerization with oxygen even in the presence of oxygen, but instead it homopolymerized to form highly crystalline homopolymer. The difference in the solid-state polymerization reactivity was discussed on the basis of molecular packing in the crystals obtained by X-ray crystallography. In addition, it was found by ESR measurement that the solid-state alternating copolymerizations with molecular oxygen proceed by means of a radical mechanism.

Preparation of Mechanically Cross-Linked Poly(vinyl alcohol), Masataka KUBO, Naoki HAYAKAWA, Yuya MINAMI, Masashi TAMURA, Takahiro UNO, Takahito ITOH: Polymer Bulletin 52, pp. 201-207, 2004

A novel cyclic macromonomer based on a cyclic polystyrene was prepared. Its radical copolymerization with vinyl acetate was carried out to give a mechanically cross-linked poly(vinyl acetate) which was converted to a mechanically cross-linked poly(vinyl alcohol) with high swellability.

Polymer Electrolytes Plasticized With Hyperbranched Polymer For Lithium Polymer Batteries, Takahito ITOH, Seiji HORII, Shinya HASHIMOTO, Takahiro UNO, Masataka KUBO: Ionics 10, pp. 450-457, 2004

Hyperbranched polymers (HBPs) with different terminal groups and different ethylene oxide (EO) chain lengths were prepared, and the influence of the HBP structures including molecular weights and molecular weight distribution on the ionic conductivity and the mechanical property of the composite polymer electrolytes composed of poly(ethylene oxide) (PEO), HBP, $BaTiO_3$ as a ceramic filler, and $Li(CF_3SO_2)_2$ as a lithium salt were investigated. It was found that the molecular weights of the HBP do not affect significantly the ionic conductivity, but the molecular weight distribution might affect it, and also further branching at the terminals of the HBP led to decrease in the ionic conductivity. The HBP with longer EO chain length was effective for enhancement of the ionic conductivity in comparison with the HBP with shorter one. The increase in cross-linkable groups (acryloyl group) at the terminals of the HBP improved the tensile strength, but caused the ionic conductivity to decrease. Loosely cross-linked composite polymer electrolyte showed higher ionic conductivity and higher tensile strength than no cross-linked one.

Double Nucleophilic Addition of Azide and Tetraallyltin to the Latent *α,β*-Unsaturated Aldehydes Using in situ Hydrolysis of the Imino Functionality Promoted by Tin(IV) Chloride Pentahydrate, Makoto SHIMIZU, Takafumi NISHI: Synlett, pp. 889-891, 2004

Double Nucleophilic Addition of Azide and Tetramethallyltin to *α,β*-Unsaturated Aldimines Promoted by Aluminum Chloride, Makoto SHIMIZU, Chiaki YAMAUCHI, Toshiki OGAWA: Chem. Lett. 33 (5), pp. 606-607, 2004

Synthesis of 5-Acetyl-2-pyridones via Nucleophilic Addition of *β*-Keto Esters to Alkynyl Imines, Iwao HACHIYA, Kana OGURA, Makoto SHIMIZU: Synthesis, pp. 1349-1352, 2004

Stereodivergent Synthesis of (*2R*)-2,3-Diricinolein by Lipase-catalyzed Hydrolysis of Triricinolein, Iwao HACHIYA, Akihisa MAKINO, Makoto, SHIMIZU, Masatsugu AKITA*, Takashi HAMAGUCHI*: Tetrahedron: Asymmetry 15 (16), pp. 2451-2454, 2004

Aza-Reformatsky-type Reaction of *α*-Iodomethyl Ketone *O*-Alkyl Oximes Promoted by Titanium Tetraiodide, Makoto SHIMIZU, Tadahiro TOYODA: Org. Bio. Chem. 2 (20), pp. 2891-2892, 2004

A Cation-Exchange Resin Promoted Imino Aldol Reaction, Leading to the Synthesis of 2-Isocephem and 2-Oxa-isocephem , Makoto SHIMIZU, Masanori TACHI, Iwao HACHIYA: Chem. Lett. 33 (10), pp. 1394-1395, 2004

An Improved Process for the Large-Scale Preparation of Antirheumatic Agent MX-68, Noriaki MARUYAMA, Hirohito SHIMIZU*, Takashi SUGIYAMA*, Masashi WATANABE*, Masahiro KATO*, Makoto SHIMIZU: Organic Process Research & Development 8 (6), pp. 883-888, 2004

Reductive Coupling of Aldehydes with Nitriles Promoted by Titanium Tetraiodide, Makoto SHIMIZU, Hiroshi GOTO: Lett. Org. Chem. 1 (4), pp. 346-348, 2004

3,4,6-Trisubstituted-2-pyrone Synthesis via the Nucleophilic Addition of 2-Alkyl Meldrum's Acid to Alkynyl Ketone, Iwao HACHIYA, Hitoshi SHIBUYA, Kazuma HANAI, Makoto SHIMIZU: Lett. Org. Chem. 1 (4), pp. 349-352, 2004
Double Nucleophilic Addition of Ketene Silyl Acetals to *α,β*-Unsaturated Imines: Factors Controlling the Regioselectivity, Makoto SHIMIZU, Hiroshi KUROKAWA, Atsushi TAKAHASHI: Lett. Org. Chem. 1 (4), pp. 353-356, 2004.

New Synthetic Reactions Using the Reducing Ability of Titanium Tetraiodide [in Japanese], Makoto SHIMIZU: J. Synth. Org. Chem., Jpn. 62 (3), pp. 205-213, 2004

Elimination-Addition Mechanism for Nucleophilic Substitution Reaction of Cyclohexenyl Iodonium Salts and Regioselectivity of Nucleophilic Addition to the Cyclohexyne Intermediate, Morifumi FUJITA*, Wan Hyeok KIM*, Yuichi SAKANISHI*, Koji FUJIWARA*, Sayaka HIRAYAMA*, Tadashi OKUYAMA*, Yasuhiro OHKI*, Kazuyuki TATSUMI*, Yasunori YOSHIOKA : J. Am. Chem. Soc. 126 (24), pp.7548-7558, 2004

The reaction of 4-substituted cyclohex-1-enyl(phenyl)iodonium tetrafluoroborate with tetrabutylammonium acetate gives both the *ipso* and *cine* acetate-substitution products in aprotic solvents. The isomeric 5-substituted iodonium salt also gives the same mixture of the isomeric acetate products. The reaction is best explained by an elimination-addition mechanism with 4-substituted cyclohexyne as a common intermediate. The cyclohexyne formation was confirmed by deuterium labeling and trapping to lead to [4 + 2] cycloadducts and a platinum-cyclohexyne complex. Cyclohexyne can also be generated in the presence of some other mild bases such as fluoride ion, alkoxides, and amines, though amines are less effective bases for the elimination. Kinetic deuterium isotope effects show that the anionic bases induce the E2 elimination ($k_H/k_D > 2$), while the amines

allow formation of a cyclohexenyl cation in chloroform to lead to E1 as well as S_N1 reactions ($k_H/k_D \approx 1$). Bases are much less effective in methanol, and methoxide was the only base to efficiently afford the cyclohexyne intermediate. Nucleophiles react with the cyclohexyne to give regioisomeric products in the ratio dependent on the ring substituent. The observed regioselectivity of nucleophilic addition to substituted cyclohexynes is rationalized from calculated LUMO populations, which are governed by the bond angles at the acetylenic carbons: The less deformed carbon has a higher LUMO population and is preferentially attacked by the nucleophile.

Vibrational Analysis with the Symmetrically Combined Morse Potential Model for Antisymmetric Stretching in [ClDCl] Formed by Photodissociation of $(DCl)_2$, Masaki MITANI, Yasunori YOSHIOKA, Dock–Chil CHE*, Toshio KASAI* : J. Phys. Chem. A 108 (24), pp.5220-5225, 2004

We estimate the line spacing between vibrational levels for the antisymmetric stretching in [ClDCl] to elucidate the origin of the oscillating structure on the translational energy distribution of the terminal D atom released by the photodissociation of $(DCl)_2$. The vibrational analysis with the symmetrically combined Morse potential model is performed for linear hydrogen-bonding [ClDCl] and the dependence of change in vibrational levels on the Cl–Cl distance is examined. It is found that the calculated assignment and observed spacing show good correspondence for R_{ClCl} = 3.65 or 3.70 Å, and it is therefore strongly suggested that the oscillation of dissociated D translational energy reflects the antisymmetric stretching vibration in the [ClDCl] counterpart.

Effect of Aging on Conductivity of Yttria Stabilized Zirconia, Masatoshi HATTORI*, Yasuo TAKEDA, Yoshinori SAKAKI*, Akihiro NAKANISHI*, Satoshi OHAR*, Kazuo MUKAI*, Jin-Ho LEE*, Takehisa FUKUI*: Journal of Power Sources 126, pp.23-27, 2004
Effect of Annealing on the Electrical Conductivity of the Y_2O_3-ZrO_2 System, M. HATTORI*, Y. TAKEDA, J. –H. LEE*, S. OHARA*, K. MUKAI*,T. FUKUI*, S. TAKAHASHI*, Y. SAKAKI*, A. NAKANISHI*: Journal of Power Sources 131, pp.247-250, 2004

The Effect of Doped Elementals on the Electrochemical Behavior of Hexagonal $Li_{2.6}Co_{0.4}N$, Yu LIU, Kumi HORIKAWA, Minako FUJIYOSHI, Nobuyuki IMANISHIi, Atsushi HIRANO, Yasuo TAKEDA: Journal of the Electrochemical Society 151(9), pp. A1450-A1455, 2004

Lithium Transition Metal Nitrides with the Modified Morphology Characteristics as Advanced Anode Materials for Lithium Ion Batteries, Y. LIU, T. MATSUURA, N. IMANISHI, T. ICHIKAWA, A. HIRANO, Y. TAKEDA: Electrochemistry Communication 6, pp.632-636, 2004

Silicon/Carbon Composites as Anode Materials for Li-Ion Batteries, Y. LIU, K. HANAI, J. YANG*, N. IMANISHI, A. HIRANO, Y. TAKEDA: Electrochemical and Solid-State Letters 7(10), pp.A369-A372, 2004

Study of the Capacity Fading Mechanism for Fe-Substituted $LiCoO_2$ Positive Electrode, Victoria L. MCLAREN*, Anthony R. WEST*, Mitsuharu TABUCHI*, Akiko NAKASHIMA*, Hikari TAKAHARA*, Hironori KOBAYASHI*, Hikari SAKAEBE*, Hiroyuki KAGEYAMA*, Atsushi HIRANO, Yasuo TAKEDA: Journal of the Electrochemical Society 151(5), pp. A672-A681, 2004

Novel Composite Anodes Based on Layered Lithium Transition Metal Nitrides for Lithium Secondary Batteries, Y. LIU, K. HORIKAWA, M. FUJIYOSHI, T. MATSUURA, N. IMANISHI, Y. TAKEDA: Solid State Ionics 172, pp.69-72, 2004

Electrical and Thermal Properties of Dense $Ce_{1-x}RE_xO_{2-\delta}$ Electrolyte Using Low-Temperature Sinterable Powder ($0 \leq x \leq 0.2$, RE=Y, Sm, Gd), Eisaku SUDA*, Bernard PACAUD*, Yvan MONTARDI*, Masashi MORI*, Yasuo TAKEDA: Transactions of the Materials Research Society of Japan 29(5), pp.2317-2320, 2004

Impedance Spectroscopy of Perovskite Air Electrodes for SOFC Prepared by Laser Ablation Method, N. IMANISHI, T. MATSUURA, Y. SUMIYA, K. YOSHIMURA, A. HIRANO, Y. TAKEDA, D. MORI*, R. KANNO*: Solid State Ionics 174, pp.245-252, 2004

Effects of Charge Disproportionation on the Phonon Density of State in Fe Perovskites, Jobu MATSUO*, Makoto SETO*, Shinji KITAO*, Yasuhiro KOBAYASHI*, Rie HARUKI*, Takaya MITSUI*, Atsushi FUJIMORI*, Yasuo TAKEDA, Shuji KAWASAKI*, Mikio TAKANO*: Journal of the Physical Society of Japan 73 (10), pp.2768-2770, 2004

Modification of Carbon Nanotubes by Laser Ablation of Copper, Akira. KOSHIO, Mitsuru SHIRAISHI, Yuuji KOBAYASHI, Masatou ISHIHARA*, Yoshinori KOGA*, Syunji BANDOW*, Sumio IIJIMA*, Fumio KOKAI: Chem. Phys. Lett. 396, pp.410-414, 2004

Multi-wall carbon nanotubes (MWNTs) were modified by laser ablation of Cu in the presence of He gas. Quasi-spherical particles with diameters of 200 nm to 2 μm were sparsely deposited on as-grown MWNTs. Agglomerated nanoparticles with sizes of 1-10 nm covered ultrasonically-treated MWNTs. Both particles were oxidized. The interaction of nanoparticles with the surface of the ultrasonicated MWNTs, due to small charge transfer to carbon atoms of the MWNTs upon adsorption of Cu, was suggested. We discuss the size distribution and morphology of the particles from cluster and particle formation in gas-phase and the surface properties of the two MWNTs.

Compression of Polyhedral Graphite up to 43 GPa and X-ray Diffraction Study on Elasticity and Stability of the Graphite Phase, Atsuko NAKAYAMA*, Sumio IIJIMA*, Yoshinori KOGA*, Katsuya SHIMIZU*, Kaori HIRAHARA*, Fumio KOKAI: Appl. Phys. Lett. 84, pp. 5112-5114, 2004

The crystal structure of polyhedral graphite particles ("G balls") has been investigated under pressure up to 43 GPa and at room temperature by x-ray powder diffraction measurements. The polyhedra maintain the graphite phase under pressure higher than 40 GPa. A 29% compression in volume at 43 GPa involves an unusual decrease in the interlayer distance of 25%. The polyhedra recover their original crystal structure by releasing the pressure. A closed and solid structure of the polyhedra, suppressing a transition into another phase, causes them to become metallic under pressure higher than 20 GPa.

Three Nanostructured Graphitic Particles and their Growth Mechanisms from High-Temperature Carbon Vapor Confined by Ar Gas, Fumio KOKAI, Akira KOSHIO, Daisuke KASUYA*, Kaori HIRAHARA*, Kunimitsu TAKAHASHI*, Atsuko NAKAYAMA*, Masatou ISHIHARA*, Yoshinori KOGA*, Sumio IIJIMA*: Carbon, 42, pp.2515-2520, 2004

CO_2 laser vaporization of graphite was carried out in the presence of high pressure Ar gas up to 0.8 MPa. We compared transmission electron microscope images and Raman spectra of deposited particles and luminous laser plumes of vaporized and clustered carbon species. We discuss the growth mechanisms of three graphitic carbon particles, a single-wall carbon nanohorn aggregate, a platelet graphite particle, and a polyhedral graphite particle, grown depending on the confinement of the Ar atmosphere. The formation of graphitic sheet or shell structures, dependent on resident carbon densities and their temperature gradient, is thought to begin from supersaturated hot carbon vapor up to about 3000°C and lead to the growth of the three graphitic particles.

Optimization of Solar Photocatalytic Degradation Conditions of Bisphenol A in Water Using Titanium Dioxide, Satoshi KANECO, Mohammad A. RAHMAN, Tohru SUZUKI, Hideyuki KATSUMATA, Kiyohisa OHTA: J. Photochem. Photobiol. A: Chem. 163, pp. 419–424, 2004

Solar Photocatalytic Degradation of Bisphenol A in Water with ZnO, Mohammad A. RAHMAN, Satoshi KANECO, Tohru SUZUKI, Hideyuki KATSUMATA, Kiyohisa OHTA: Photo/Electrochem. Photobiol. Environ. Energy Fuel 3, pp. 199–205, 2004

Determination of Silver in Waters by Tungsten Wire Preconcentration Method - Electrothermal Atomic Absorption Spectrometry, Mohammad A. RAHMAN, Satoshi KANECO, Md N. AMIN, Tohru SUZUKI, Kiyohisa OHTA: Talanta 62, pp. 1047–1050, 2004

Separation of Zinc Compounds by Sequential Metal Vapor Elution Analysis with Atomic Absorption Detection, Mohammad A. RAHMAN, Satoshi KANECO, Tohru SUZUKI, Hideyuki KATSUMATA, Kiyohisa OHTA: Talanta 64, pp. 989–992, 2004

Slurry Sampling for Direct Analysis of Lead in Bangladeshi Vegetable Samples by Molybdenum Electrothermal Atomizer Atomic Absorption Spectrometry, Mohammad A. RAHMAN, Satoshi

KANECO, Tohru SUZUKI, Hideyuki KATSUMATA, Kiyohisa OHTA: ITE Lett. Batt. New Technol. Med. 5, pp. 363–368, 2004

Leaching Behavior of Lead Compounds in Atmosphere Fine and Coarse Particles, Kunihiro FUNASAKA*, Takeji MIYAZAKI*, Toshikazu KAMIURA*, Joji FUKUYAMA*, Hideyuki KATSUMATA, Satoshi KANECO, Tohru SUZUKI, Kiyohisa OHTA: ITE Lett. Batt. New Technol. Med. 5, pp. 577–580, 2004

Development of Sintering Preparation Technology of Porous Materials from Sea Bottom Sediments for Waste Water Treatment, Satoshi KANECO, Takuya HARADA, Ahmed H.A. DABWAN, Tohru SUZUKI, Hideyuki KATSUMATA, Kiyohisa OHTA: ITE Lett. Batt. New Technol. Med. 5, pp. 467–471, 2004

Electrochemical Reduction of CO_2 at Alloy Electrode in Methanol, Satoshi KANECO, Hiroki YAMAUCHI, Hideyuki KATSUMATA, Tohru SUZUKI, Kiyohisa OHTA: Stud. Surf. Sci. Catal. 153, pp. 277–282, 2004

Reduction of Carbon Dioxide Using Metal Powders, Hideyuki KATSUMATA, Kouichirou MATSUSHITA, Satoshi KANECO, Tohru SUZUKI, Kiyohisa OHTA: Stud. Surf. Sci. Catal. 153, pp. 55–60, 2004

Long Term Sampling Method for PCDD/Fs in Atmosphere by Adsorption onto Economical Materials, Hideyuki KATSUMATA, Satoshi KANECO, Tohru SUZUKI, Kiyohisa OHTA: Chem. Lett. 33, pp. 1618–1619, 2004

Effect of Metal Nitrates on the Formation of PCDD/Fs during Newspaper Combustion, Hideyuki KATSUMATA, Satoshi KANECO, Tohru SUZUKI, Kiyohisa OHTA: Bull. Environ. Contamn. Toxicol. 73, pp. 479–486, 2004

Removal of Humic Substances and Their Metal Complexes by Adsorption with Bone Char, Hideyuki KATSUMATA, Satoshi KANECO, Haruna KASAI, Kumiko ITOH, Kazuaki MASUYAMA*, Tohru SUZUKI, Kunihiro FUNASAKA*, Kiyohisa OHTA: Environ. Eng. Sci. 21, pp. 341–348, 2004

Microbial Metabolism of Di-*n*-Butyl Phthalate by Bacterium *Bacillus Natto*, Aleya BEGUM, Hideyuki KATSUMATA, Satoshi KANECO, Tohru SUZUKI, Kiyohisa OHTA: Chem. Lett. 33, pp. 682–683, 2004

Removal of Heavy Metals in Aqueous Solution by Adsorption onto Oyster Shell, Hideyuki

KATSUMATA, Satoshi KANECO, Tohru SUZUKI, Kiyohisa OHTA, Yoshihiro YOBIKO: Photo/Electrochem. Photobiol. Environ. Energy Fuel 3, pp. 165–172, 2004

Removal of Heavy Metals in Water by Adsorption onto Sintering Porous Materials from Sea Bottom Sediments, Hideyuki KATSUMATA, Takuya HARADA, Satoshi KANECO, Ahmed H.A. DABWAN, Tohru SUZUKI, Kiyohisa OHTA: ITE Lett. Batt. New Technol. Med. 5, pp. 573– 576, 2004

Preconcentration of Phthalic Acid Esters in Water Samples by *Saccharomyces cerevisiae* Immobilized on Silica Gel, Hideyuki KATSUMATA, Aleya BEGUM, Satoshi KANECO, Tohru SUZUKI, Kiyohisa OHTA: Anal. Chim. Acta 502, pp. 167–172, 2004

Degradation of Bisphenol A in Water by the Photo-Fenton Reaction, Hideyuki KATSUMATA, Shinsuke KAWABE, Satoshi KANECO, Tohru SUZUKI, Kiyohisa OHTA: J. Photochem. Photobiol. A: Chem. 162, pp. 297–305, 2004

Nucleotide Sequence Analysis of *p10* Gene of *Antheraea pernyi* Nucleopolyhedrovirus and Construction of Two Transfer Vector Plasmids, Kenichi MAEGAWA, Xie T. WANG*, Jun KOBAYASHI*, Tetsuro YOSHIMURA: International Journal of Wild Silkmoth and Silk 9, pp. 53-60, 2004

Development of Orally Administrated Liposome Vaccines against Bacteria- and Virus-Infectious Diseases in Cultured Fishes: Tetsuro YOSHIMURA, Takeyoshi TAKAGI, Kanta TSUMOTO, Masayuki SHONO, Teruo MIYAZAKI: Immunology 2004, pp. 225-228, 2004

Ligand-Printed Ion Pore Composed of Polypeptide Assembly in a Lipid Bilayer Membrane, Masahiro HIGUCHI, Tomoyuki KOGA*, Yoshiaki KOBUKE*, Takatoshi KINOSHITA*, Masami KAWAGUCHI: Trans. MRS-J. 29, pp. 3143-3146, 2004

A simple and novel approach for the preparation of a synthetic ligand-gated ion channel was investigated. The ligand-induced formation of an amphiphilic polypeptide assembly acts as an ion channel in lipid bilayer membrane. Various functional groups, which bind to the specific site on the ligand (X), were introduced at the amino terminal of α-helical polypeptide. The interaction between the ligand (X) and the terminal groups of the polypeptides induced the specific location of the α-helical polypeptide rods. Removing of the ligand (X) provided the ligand-printed ion pore in the membrane, while re-binding of the ligand (X) closed the pore. Another ligand (Y) was inactive to the ligand (X)-printed ion pore, *i.e.*, it did not close the channel. This ligand-printed polypeptide assembly may permit a novel and easier production of the ligand-gated ion channel, which will give a novel approach for the construction of signal transduction molecular devices.

Viscous Fingering of Silica Suspensions Dispersed in Polymer Fluids, Masami KAWAGUCHI: ACS Symposium Series No. 869 Nonlinear Dynamics in Polymeric Systems, pp. 250-261, 2004

Experimental studies of the viscous fingering of shear shinning silica suspensions in a radial Hele-Shaw cell and shear thickening silica suspensions in a linear Hele-Shaw cell were performed by the injection of air. For the shear thinning silica suspensions, the instability, namely changes in the viscous fingering pattern, was strongly related to the polymer concentration in the dispersant rather than the silica concentration. For the shear thickening silica suspensions, the imposed shear rate at which the instability was first observed, was close to the critical shear rate of the corresponding silica suspension. The finger velocities of the shear thinning silica suspensions were in agreement with the modified Darcy's law, while those of the shear thickening silica suspensions with the silica concentrations higher than 7.5 wt% were much lower than the prediction of the modified Darcy's law.

Rheo-Optical Properties of Silicone Oil Emulsions in the Presence of Polymer Emulsifiers, Masami KAWAGUCHI, Kenji KUBOTA: Langmuir 20 (4), pp. 1126-1129, 2004

Oil in water emulsions were prepared by dispersion of silicone oils into an aqueous solution of hydroxylpropyl methyl cellulose (HPMC) or poly(ethylene oxide) (PEO)-poly(propylene oxide) (PPO)-PEO block copolymers. The emulsions were characterized by measurements of steady-state shear viscosities, dynamic moduli, and stress-strain sweep curves coupled with optical microscope observation. The emulsions emulsified by HPMC showed solid-like viscoelastic responses, while the emulsions prepared by the block copolymers indicated liquid-like viscoelastic behavior. The simultaneous optical microscopic observation showed that the emulsions stabilized by HPMC did not flow below the yield stress, while those by the block copolymers did flow.

Viscous Fingering Instabilities in an Oil in Water Emulsion, Masami KAWAGUCGHI, Sayaka YAMAZAKI, Tadaya KATO: Phys. Fluids 16 (6), pp. 1908-1914, 2004

Viscous fingering of silicone oil emulsion stabilized by hydroxylpropyl methyl cellulose (HPMC) in water was performed by the injection of water and an aqueous solution of HPMC as a function of the injection rate. The pressure imposed at the finger tip was simultaneously monitored. Changes in the viscous fingering patterns from a crack-like pattern to a ramified one through a cups-like one were observed with an increase of the injection rate, irrespective of the injected fluid. Such a pattern transition was strongly related to rheological properties of the emulsion. Moreover, the finger velocities of the emulsion were in agreement with the modified Darcy's law

Structure Study of Binary Titanophosphate Glasses Prepared by Sol-Gel and Melting Methods, Anjiang TANG, Tadanori HASHIMOTO, Tetsuya NISHIDA, Hiroyuki NASU, Kanichi KAMIYA: Journal of the Ceramic Society of Japan 112(9), pp. 496-501, 2004

The $70TiO_2 \cdot 30P_2O_5$ (mol%) glass was prepared by the sol-gel method. Its structure was examined by means of IR, Raman spectroscopy and X-ray radial distribution function analysis, and was compared with the corresponding melt-derived glass. It was found that average coordination number of Ti^{4+} ions was almost 6 and Ti^{4+} ions formed predominantly TiO_6 octahedra in the

sol-gel-derived glass, while Ti^{4+} ions were present in the 4, 5 and / or 6-fold coordination states to give average coordination number in-between 4 and 5 in the melt-glass. The preference of high coordination state of Ti^{4+} ions in the sol-gel glass was consistent with higher refractive index and density than the melt-glass.

Effective Deposition of Nano-Sized Silver Particles on Silica to Develop a Sensitive Local Plasmon-Based SPR Sensor, Noritsugu HASIMOTO*, Tadanori HASHIMOTO, Koichi MORI, Hiroyuki NASU, Kanichi KAMIYA: Journal of the Ceramic Society of Japan, Supplement 112-1, PacRim5 Special Issue 112(5), pp. S576-S578, 2004

Nano-sized silver particles-deposited silicas were prepared by (a) the sol-gel method, the evaporation-condensation of silver on (b) silica glass and (c) sol-gel derived silica film. Optical absorption peak due to surface plasmon resonance (SPR) of silver particles was measured using UV-VIS spectrophotometer. When the films were immersed in liquid, SPR absorption peak of the films (b) and (c) was shifted toward longer wavelength with the increase of the refractive index of the liquid, suggesting that these films can be used as optical sensors. On the other hand, SPR absorption peak of the film (a) was little shifted. The sensitivity to the refractive index change for the film (b) was 81.4 nm, and that of the film (c) made by depositing silver particles on the sol-gel silica was large as 90.2 nm, which may be attributed to less coverage of silver particles with silica matrix than the film (a) and less aggregate of them than the film (b).

Optical Properties of Ti^{3+}-Free Ternary Titanophosphate Glasses, Tadanori HASHIMOTO, Hiroyuki NASU, Kanichi KAMIYA: Proceedings of the XX ICG in Kyoto, Sep.27th-Oct.1st, O-07-085, 2004

The Ti^{3+}-free binary TiO_2-P_2O_5 glasses containing TiO_2 up to 74 mol% prepared by the melt-quenching and a long-term post-annealing around the glass transition temperature in the air possess high transparency, high-index, high-dispersion and low density, and are expected as novel eco-optical glasses. In the present study, the effect of third and fourth components on the time of post-annealing to remove Ti^{3+} ions, and linear and nonlinear optical properties was examined. The substitution of K_2O for P_2O_5 in binary glasses shortened the post-annealing time and decreased the thermo-optic coefficient. The addition of a small amount of SnO_2 to binary glasses was found to be effective for removing Ti^{3+} ions, or decoloration of glasses with maintaining high-index, and also for stabilizing laser pulses. In addition, quaternary Li_2O-ZnO-TiO_2-P_2O_5 glasses were expected as high-index molding glasses.

Structure Study of TiO_2-P_2O_5 Glasses Prepared by Sol-Gel Method, Anjiang TANG, Tadanori HASHIMOTO, Hiroyuki NASU, Kanichi KAMIYA: Proceedings of the XX ICG in Kyoto, Sep.27th-Oct.1st, O-10-021, 2004

The $xTiO_2 \cdot (100\text{-}x)P_2O_5$ (x = 70-95 mol%) glasses with refractive indicies as high as 2.1-2.3 were prepared by the sol-gel method. The refractive index was higher in the sol-gel-glass than in the melt-glass at x = 70. Heat-treated compositions with x = 90 and 95 were considered to be composites of 13-15 mass% nano-sized anatase and glass matrices with x slightly smaller than nominal values,

but were highly transparent. It was found by IR and Raman techniques that 6-fold coordinated Ti^{4+} ions are predominant in the glass phase, while 4 or 5, and 6-fold ones are coexisting in the melt-glass of x = 70. These results were consistent with very high refractive index of the sol-gel glasses.

Influences of Nanocrystal-Size and Matrix on Third-Order Optical Nonlinearity for Thin Films Prepared by RF-Sputtering, Hiroyuki NASU, Akimasa TANAKA, Tadanori HASHIMOTO, Kanichi KAMIYA, Kenji KAMADA*: Proceedings of the XX ICG in Kyoto, Sep.27th-Oct.1st, O-16-017, 2004

CdSe microcrystals with various size was successfully embedded in various glass matrices by magnetron Rf sputtering technique. The mean size of microcrystals was controllable by changing the relative surface ratio of CdSe pellets to the matrix in the target, and increased with increasing the relative area. The negative real part of the third-order optical susceptibility was seen for the all present films, and magnitude of the absolute value of real part in the same glass matrix increased with decreasing microcrystal size. On the other hand, the increase of the dielectric constant of the matrix increase the magnitude. Therefore it is interpreted that the strengthening the quantum size effect increase the magnitude of the real part of the third-order optical nonlinearity. Furthermore, even taking account of the imaginary part, it is evident that the strengthening the quantum size effect increases total third-order optical nonlinearity.

Electroluminescence from CdSe Nanocrystal-Doped ITO Films on SiO_2 Glass Substrates, Hiroyuki NASU, Yasuhiro Matsuzaki, Tadanori HASHIMOTO, Kanichi KAMIYA: Proceedings of the XX ICG in Kyoto, Sep.27th-Oct.1st, O-16-025, 2004

Electroluminescence was observed in CdSe microcrystal-doped indium tin oxide (ITO) thin films on SiO_2 glass substrates by Rf-sputtering method. The size of CdSe microcrystals was changed by altering the relative surface area of the CdSe pellets on the ITO target. ITO was well crystallized on SiO_2 glass substrates. Emission spectra shifted from red to yellow with decreasing CdSe microcrystal size. The shift was considered to result from the blue shift of the absorption edge caused by the quantum confinement effect of CdSe microcrystals.

Review of Combination of Peritoneal Dialysis and Hemodialysis as a Modality of Treatment for End-stage Renal Disease, H. FUKUI*, S. HARA*, Y. HASHIMOTO*, T. HORIUCHI, M. IKEZOE*, N. ITAMI*, M. KAWABE*, H. KAWANISHI*, Y. KIMURA*: Ther Apher Dial 8, pp. 56-61, 2004

Because the contribution of residual renal function (RRF) to total solute clearance is often significant in continuous ambulatory peritoneal dialysis (CAPD), loss of RPF over time can lead to inadequate dialysis if appropriate prescription management strategies are not pursued. Additionally, declines in ultrafiltration caused by increases in peritoneal permeability may limit continuation of CAPD therapy. Peritoneal dialysis and hemodialysis (PD+HD) combination therapy (complementary dialysis therapy) is an alternative method. This therapy allows the patient to maintain daily activities, as with CAPD, while undergoing once-a-week HD supplements for the insufficient removal of solutes and water. This therapy allows for the continuation of PD without shifting to total HD in PD patients who continue to have uremic symptoms even after individualization of the PD prescription.

This treatment option is psychologically more acceptable to patients and may be expected to provide such accompanying beneficial effects as peritoneal resting, impravement of QOL and reduction in medical cost.

Department of Architecture

*nonmember

Characteristics of The Learning Room Use of Environmental Education Facilities from the Viewpoint of Learning Programs Execution - A Study on The Relation between Learning room/equipments and Learning Programs at Environmental Education Facilities Part1-[in Japanese], Hiroki OGAWA and Masuro URAYAMA, Journal of Architecture and Planning, No.581, pp.33-40, 2004.7

This paper clarifies the relation between learning rooms and learning programs of environmental education facilities. Main results are as follow;
1. There are many learning programs of interest or knowledge stage, and a few one of action or understanding stage. Many facilities carry out programs of the only interest stage. But more than half execute learning programs which have a combination of some aim stages.
2. From the equipments of learning room, the use form of leaning room is classified in lecture, training, teaching materials and exhibition. Learning programs of using the plural room are able to achieve a higher stage than ones of the single room use.

A Study on Forming Civic Center and Urban Renewal in Prefectural Capital Cities based on Japanese Castle-Towns in the Meiji and Taisho era. [in Japanese], Kenjiro MATSUURA, Yoshihiro YOKOTA , Satoshi KUSAKABE , Masuro URAYAMA and Shigeru SATOH : Jounal of Architecture and Planning , Transactions of Architectural Institute of Japan, No. 581, p.p. 67-74, 2004. 7

This paper aims to clarify how to form Civic Center for Urban Renewal analyzing cases of prefectural capital 27 Cities based on Japanese Castle-Towns in the Meiji and Taisho era.

Findings are as follows : 1) Government and municipal offices tended to be nearby castle and gather each other to form Civic Center , 2)Just after replacing feudal domain system with prefecture system and operation of city organization system , there were many cases of conversion of existing institutions to prefectural offices and city offices , 3)Nearby Civic Center , Castle Renewal such as reclaiming moats and creating new roads was done in many cities.

A Study on Visual Impacts of Windfarm -On Influences of Windmills Arrangement to Landscape Evaluation-[in Japanese], Shinjiro SAKAMOTO, Fumiko KAMIYA and Masuro URAYAMA, Papers on Environmental Information Science, No.18, pp1-6, 2004.11

The purpose of this study is to analyze visual impacts of windmills arrangement to landscape evaluation. We prepared CG pictures which were drawn in combination of layout, distance from standpoint to windmills and distance between windmills. 48 students evaluated these pictures with 10 adjective scales. We found 3 factors of landscape evaluation, and analyzed the relation between them and windmill arrangement.

MANAGEMENT OF A COMMUNITY FACILITY CONVERTED VACANT SHOP AT THE CENTRAL DISTRICT OF A LOCAL SMALL TOWN AND ITS EFFECTS -Through a social experiment at Kamiichi in Yoshino Town, Nara prefecture-[in Japanese], Hiroki KAWAKITA and Masuro URAYAMA, AIJ Journal of Technology and Design, No.20, pp. 319-324, 2004.12

As it is required to develop a management system of vacant shops at central district of local small towns, this paper reports the challenge for local residents group to convert a vacant shop to a community facility, and management of it at Kamiichi district of Yoshino Town, Nara Prefecture. This facility offered only a place to local people at beginning. After changing to sponsor various use opportunities, this came to be use positively, and made local people feel liveliness. To keep these effects, it is subject to be secured so that maintenance administrative expenses can be paid for local residents group, and attractive use opportunities can continue being sponsored.

A Study on the Transfiguration of the Landscape Ordinance in the Prefectures, Yoshio BANDO, Satoshi ASANO and Shoji IMAI, Journal of Architecture and Planning, No.578, pp.85-92, 2004

The Actual Conditions of the Acceptance and Evaluation of Users for Housing Performance Indication System (Apartment Houses) in Housing Quality Assurance Act [in Japanese], Hiroyuki Takai, Urban Housing Scieces, No.47, pp.95-100, 2004

The aim of this research is to make clear the acceptance condition and evaluation of users for Housing Performance Indication System (Apartment houses) in Housing Quality Assurance Act. The research was made for 210 residents living in the apartment houses adopted the system, and it was found that the system contributes to users ' choosing houses much. But there are some problems. For example more popularization of the system and more information easy to understand and useful to judge for users are needed.

A Study on the Successive Change Condition of Common Facilities in Condominiums Including Many Units [in Japanese], Yuki Miyauchi , Hiroyuki Takai , Mitsuo Takada* , Hiroko Saito*, Urban Housing Scieces, No.47, pp.41-46, 2004

The aim of this research is to make clear the actual condition on successive change of common spaces and facilities in condominiums including many units. The research was made for 40 housing estates in Kansai and Tokyo Metropolitan area by the way of questionnairs to the chief of homeowners association or the management staff and hearing on 3 housing estates. So big change is not occurred yet, but we can find many symptoms. We could find variety of repeated trial and error and changes keep up with an aging repairs costs and management costs.

Improvement of Quality of Concrete with Permeable Form [in Japanese], Naoki MISHIMA, Shigemitsu HATANAKA, Hiromi KOBAYASHI* and Toshitsugu INUKAI, Proceedings of the

Japan Concrete Institute, Vol.26, No.1, pp.363-368, 2004.7

Influence of Magnitude of Pressure for Vacuum Processing on Strength Distribution in Concrete Slab [in Japanese], Hiroshi WATO, Shigemitsu HATANAKA, Naoki MIAHIMA and Akio MURAMATSU*, Proceedings of the Japan Concrete Institute, Vol.26, No.1, pp.375-380, 2004.7

Fundamental Study on Bleeding Behavior in Concrete by Visible Evaluation Method [in Japanese], Toshitsugu INUKAI, Shigemitsu HATANAKA, Naoki MISHIMA and Rinji KANEKO*, Proceedings of the Japan Concrete Institute, Vol.26, No.1, pp.609-614, 2004.7

Fundamental Study on Compaction Mechanism Based on the Consolidation Theory [in Japanese], Hiroki HATTORI, Shigemitsu HATANAKA, Eisuke SAKAMOTO and Naoki MISHIMA, Proceedings of the Japan Concrete Institute, Vol.26, No.1, pp.1227-1232, 2004.7

Visualized Experiment on Air Bubbles Behavior in Concrete of Vacuum-processed Process [in Japanese], Eisuke SAKAMOTO, Shigemitsu HATANAKA, Hiroki HATTORI and Naoki MISHIMA , Proceedings of the Japan Concrete Institute, Vol.26, No.1, pp.1233-1238, 2004.7

Influence of Paste Strength on Compressive Strength of Porous Concrete [in Japanese], Yukihisa YUASA*, Shigemitsu HATANAKA, Naoki MISHIMA and Ken MURAO*, Proceedings of the Japan Concrete Institute, Vol.26, No.1, pp.1425-1430, 2004.7

Fundamental Study on Manufacture of Large Particle Porous Concrete Using Concrete Rubble [in Japanese], Akihiro MAEGAWA, Shigemitsu HATANAKA, Naoki MISHIMA and Yukihisa YUASA*, Proceedings of the Japan Concrete Institute, Vol.26, No.1, pp.1455-1460, 2004.7

Uniaxial Compression 3-D FEM Analysis of Cylindrical Concrete Specimens with Different Shape Ratios [in Japanese], Yukio YOSHIDA, Eiji MIZUNO* and Shigemitsu HATANAKA, Proceedings of the Japan Concrete Institute, Vol.26, No.2, pp.19-24, 2004.7

Analytical Study on Confining Effect Inside Confined Concrete Subjected to Axial Compressive Force [in Japanese], Makoto ITO*, Eiji MIZUNO* and Shigemitsu HATANAKA, Proceedings of the Japan Concrete Institute, Vol.26, No.2, pp.31-36, 2004.7

Fundamental Study on Rotation Condition of Shear Wall in Seismic Evaluation of RC Buildings [in Japanese], Kenzo KUBOTA Shigemitsu HATANAKA and Yoshiyuki KATO*, Proceedings of the Japan Concrete Institute, Vol.26, No.2, pp.1327-1332, 2004.7

Fundamental Study on Compaction Mechanism of Vacuum Processing Method Based on the Consolidation Theory [in Japanese], Hiroki HATTORI, Shigemitsu HANATANA, Naoki MISHIMA and Eisuke SAKAMOTO, J. Struct. Constr. Eng. AIJ, No.585, pp.7-13, 2004.11

The strength and hardness of concrete slab surface is considered significantly affected by bleeding of concrete. It has been reported that dewatering by vacuum processing is quite effective to make concrete high density and high strength. The method, however, has not been successfully used for the concrete works in the field of building construction, compared with that of civil engineering works in Japan. In the earlier report, the authors have already pointed out that there is a strong relationship between the strength distribution and density distribution in the vacuum processed concrete, both gradually decreasing from the top surface to about 15 cm depth of concrete. Main purpose of the present study is to discuss the mechanism of the occurrence of such distribution of strength and density, based on consolidation theory. In the experiment, pore water pressure distribution in concrete has been measured using the original measuring system. As a result, it has been confirmed that the consolidation theory is quite effective to explain the internal properties of vacuum processed concrete as well as those of press-dewatered concrete.

EXPERIMENTAL STUDY ON ELASTICS-PLASTIC BEHAVIOR AND ULTIMATE STRENGTH OF EXPOSURE FIXED-TYPE STEEL COLUMN-BASE SUBJECTED TO BENDING MOMENT [in Japanese], Haruyoshi Kadoya*, Jun Kawaguchi and Shosuke Morino, Journal of Structural and Construction Engineering, Number 583, pp.123-130, 2004.9.

Experimental Study on Strength and Stiffness of Bare Type CFT Column Base with Central Reinforcing Bars, Haruyoshi Kadoya*, Jun Kawaguchi and Shosuke Morino, COMPOSITE CONSTRUCTION IN STEEL AND CONCRETE V, pp.1-10, 2004.

Dynamic response of steel beam-columns with square hollow section - Shaking table tests of steel beam-columns subjected to biaxial bending (part 1), Yasuhiro Uchida*, Jun Kawaguchi and Shosuke Morino, Journal of Structural and Construction Engineering, Number 577, pp.123-130, 2004.3.

Structural design of frame structures by means of a multiobjective genetic algorithm, Toyofumi TAKADA and Keigo MATSUSHIMA, Proc. of the 4th Int. Conf. on Engineering Computational Technology (CD-ROM), paper 104, 2004

Simplified Design Method for Air-based Solar Heating System [in Japanese], Hiroaki KITANO and Kazunobu SAGARA*, Journal of Enviromental Engineering, No.582, pp.45-52, 2004.8

Reducing Effect of Fresh Air Latent Heat Load in Air to Earth Heat Exchange using Underground Double Floor Space, Wontug SON, Hisaya NAGAI, Journal of Asian Architecture and Building Engineering, Vol.3, No.2,pp.29-34, 2004

Department of Information Engineering

*nonmember

The Joinability and Unification Problems for Confluent Semi-Constructor TRSs , Ichiro MITSUHASHI, Michio OYAMAGUCHI, Yoshikatsu OHTA and Toshiyuki YAMADA, Proceedings of the 15th International Conference on Rewriting Techniques and Applications (RTA 2004), Lecture Notes in Computer Science 3091, pp.285-300, June 2004.

The unification problem for term rewriting systems (TRSs) is the problem of deciding, for a TRS R and two terms s and t, whether s and t are unifiable modulo R. Mitsuhashi et al. have shown that the problem is decidable for confluent simple TRSs. Here, a TRS is simple if the right-hand side of every rewrite rule is a ground term or a variable. In this paper, we extend this result and show that the unification problem for confluent semi-constructor TRSs is decidable. Here, a semi-constructor TRS is such a TRS that every subterm of the right-hand side of each rewrite rule is ground if its root is a defined symbol. We first show the decidability of joinability for confluent semi-constructor TRSs. Then, using the decision algorithm for joinability, we obtain a unification algorithm for confluent semi-constructor TRSs.

Inductive Theorems for Higher-Order Rewriting, Takahito AOTO*, Toshiyuki YAMADA and Yoshihito TOYAMA*, Proceedings of the 15th International Conference on Rewriting Techniques and Applications (RTA 2004), Lecture Notes in Computer Science 3091, pp.269-284, June 2004.

Simply typed term rewriting proposed by Yamada (2001) is a framework of higher-order term rewriting which dispenses with bound variables. This paper proposes an extention of the dependency pair method of first-order term rewriting introduced by Arts and Giesl (2000), which enables automated termination proof of simply typed term rewriting systems.

Improvements on SIMD Macroblock Processor in MPEG-2Video Encoder LSI, Koyo NITTA*, Takeshi YOSHITOME*, Toshio KONDO, Hiroe IWASAKI* and Jiro NAGANUMA*: Trans. of IEICE, Vol.J87-C, No.4, pp.377-385,2004

Low Energy Consumption by a Variable Stages Pipeline Technique, Yuji Ichikawa*, Takahiro Sasaki, Tetsuo Hironaka*, Toshiaki Kitamura*, Toshio Kondo: International Technical Conference on Circuits/Systems, Computers and Communications, 2004

Proposition and Evaluation of a Bank based Multi-port Memory with Blocking Network, Tomohiro Inoue*, Tetsuo Hironaka*, Takahiro Sasaki, Seiji Fukae*, Tetsushi Koide*, Hans Jurgen Mattausch*: International Technical Conference on Circuits/Systems, Computers and Communications, 2004

Featuring vowels by five layers sandglass type neural network [in Japanese], Tadaaki SHIMIZU*,

Masaya KIMOTO*, Hiroki YOSHIMURA*, Naoki ISU, Kazuhiro SUGATA*: Brain Neural Net., Vol.11, pp.167-175, 2004.

We showed a new scheme to characterize speech from LSP parameters by 5 layers sandglass type nonlinear neural network (SNN(NL5)). In order to synthesize speech, we take advantage of useful abilities of SNN(NL5) for compressing and restoring the information. We performed learning experiments on LSP parameters of 5 vowels to investigate the ability of SNN. The followings were verified, 1) the distribution of LSP parameters compressed by SNN(NL5) are similar to the distribution of F1-F2 formants plane. 2) Nonlinear output function of neural elements in second and fourth layers of SNN(NL5) work effectively from view point of separating the distribution of vowels. 3) In order to prevent SNN(NL5) from over learning, there exists the optimum numbers of neural elements in second and fourth layers. For 14 orders of LSP parameters, this number was determined to be 20. 4) There is a preferable property on the plane to separate the vowels distinctively when the restoring error of LSP parameters becomes less. 5) SNN(NL5) can restore the LSP parameters with accuracy enough to synthesize speech from the compressed parameters.

An evaluation of question answering challenge (QAC-1) at the NTCIR workshop 3, Jun'ichi FUKUMOTO*, Tsuneaki KATO*, and Fumito MASUI: ACM SIGIR Forum, Vol.38, Issue 1, pp.25--28, 2004.6.

In this paper we describe the Question Answering Challenge (QAC), a question answering task, and its first evaluation (QAC1). The project was carried out as a task of the NTCIR Workshop 3 in October 2002. One objective of the QAC was to develop practical QA systems in a general domain by focusing on research relating to user interaction and information extraction. Our second objective was to develop an evaluation method for the question answering system and information resources for evaluation. We defined three kinds of tasks in the QAC: Task 1, where questions required five possible answers;, Task 2, where questions had a single answer; and Task 3 ,where there was one answer to a question related to a question in Task 2. We prepared 200 questions for Task 1 and Task 2 and 40 questions for Task 3 at the Formal Run and about 900 questions for the additional run. We conducted a Dry Run and a Formal Run evaluation. There were 16 participants (two of them from among the task organizers) at the QAC1.

A Method for Rating English Texts by Reading Level for Japanese Learners of English [in Japanese], Ryo NAGATA, Tatsuya IGUCHI, Fumito MASUI, and Atsuo KAWAI: IEICE Vol.J87-D-II, No.6, pp.1329--1338., 2004.6.

It has been recognized that existing methods for rating English texts by reading level are mostly aimed at native speakers of English and therefore are not completely appropriate for Japanese learners of the language. Here we propose a method for rating English texts by reading level specifically targeted at Japanese learners of the language. To rate the reading level of a text for a Japanese learner of English, our method takes two types information regarding a given text into account, namely, vocabulary and grammatical structure. Specifically, we rate the reading level of a text by using a vocabulary list and parser to extract particularly difficult vocabulary items or grammatical structures as features. To rate a text's reading level, two types of model are used:

multiple regression and neural networks. Our experiments show that the proposed methods rate the reading level of a text with the following levels of accuracy: an average of 75% accuracy for multiple regression and 81% when using neural networks.

Sensation and Illusion of Rotation Caused by a Coriolis Stimulus [in Japanese], Naoki ISU, Atsuo KAWAI, and Fumito MASUI: Equilibrium Res., Vol.63, No.3, pp.183-193, 2004.

The sensation of rotation derived from the semicircular canal system during a Coriolis stimulus, or cross-coupled rotation, was estimated by an approach from mechanics with giving some hypotheses and simplifications on the semicircular canal system. By solving an equation of motion of the endolymph during a Coriolis stimulus with a moderate time course, rotating angle of the endolymph was obtained, and the sensation of rotation derived from each semicircular canal was estimated. Then the sensation was integrated in the whole semicircular canal system which was considered to be composed of three orthogonal semicircular canals. The sensation of rotation derived from the semicircular canal system comes into conflict with those from the otolithic system and the somatosensory system. The conflict causes an illusion such that the head rotates vertically with keeping inclination at a constant tilt angle. The nauseogenic severity of motion sickness caused by a Coriolis stimulus is enhanced in accordance with the integrated angle of rotation perceived by the illusion.

Recognizing Article Errors in the Writing of Japanese Learners of English[in Japanese], Ryo NAGATA, Tatsuya IGUCHI, Kenta WAKIDERA, Fumito MASUI, and Atsuo KAWAI: IEICE Vol.J87-D-I, No.1, pp.60--68., 2004.1.

In this paper, the authors propose a method to recognize article errors often seen in English text written by Japanese learners of English. In this method, article errors are recognized based on the statistic extracted from an electronic corpus such as English-language newspapers. The authors' method is different from earlier methods in that there is no need to create a dictionary or rules for article error recognition. The results of experiments confirm that the performance of the authors' method is equivalent or superior to earlier methods.

Question Answering Method -- Answering to Questions based on Hudge Data Set -- [in Japanese], Jun'ichi FUKUMOTO* and Fumito MASUI: Information Processing Society of Japan Magazine, vol.45, No.6, pp.30--25., 2004.

Recognizing Article Errors based on the Three Head Words, Ryo NAGATA, Fumito MASUI, Atsuo KAWAI, and Naoki ISU: In Proceedings of the Cognition and Exploratory Learning in Digital Age(CELDA 2004), pp.165--172, 2004.

A Method for Distinguishing Mass and Count Nouns Based on Contextual Information, Ryo NAGATA, Fumito MASUI, Atsuo KAWAI, and Naoki ISU: In Proceedings of the 4th International Symposium

on Human and Artificial Intelligence Systems(International Series on Natural and Artificial Intelligence), pp.516--521, 2004.

MAIQA: Mie Univ. Participated System at NTCIR4 QAC2, Naoya HIDAKA and Fumito MASUI: In Working Notes of the Fourth NTCIR Workshop Meeting(NTCIR4), pp.315--319, 2004.

Question Answering Chlallenge for Information Access Dialogue -- Overview of NTCIR4 QAC2 Subtask3 --, Tsuneaki KATO*, Jun'ichi FUKUMOTO*, and Fumito MASUI: In Working Notes of the Fourth NTCIR Workshop Meeting(NTCIR4), pp.291--297, 2004.

Question Answering Callenge for Five ranked anwers and List answers -- Overview of NTCIR4 QAC2 Subtask 1 and 2 --, Jun'ichi FUKUMOTO*, Tsuneaki KATO*, and Fumito MASUI: In Working Notes of the Fourth NTCIR Workshop Meeting(NTCIR4), pp.283--290, 2004.

Handling Information Access Dialogue through QA Technologies - A novel challenge for open-domain question answering, Tsuneaki KATO*, Jun'ichi FUKUMOTO*, Fumito MASUI and Noriko KANDO*:
In Proceedings of the Workshop on Pragmatics of Question Answering at HLT-NAACL 2004, pp.70--77, 2004.

Assessment of Regional Intra-myocardial Layer Function from Ultrasonic RF echo Signal Using Hierarchical Correlation Method with Confidence, Kiyotsugu SEKIOKA*, Toshihiro KUMISADA, Shinji TSURUOKA, Hirotake ISHII, Wataru OHYAMA, and Tetsushi WAKABAYASHI: The Transactions of The Institute of Electronics, Information and Communication Engineers, Vol. J87-D-II, No.1, pp.98-108, January, 2004

Automatic text classification of English newswire articles based on statistical classification techniques, Guowei ZU, Wataru OHYAMA, Tetsushi WAKABAYASHI and Fumitaka KIMURA: The transactions of The Institute of Electrical Engineers of Japan: Vol.124-C, No.3,pp 852--860, March, 2004

Background removal for check processing using morphology, Yimei DING, Fumitaka KIMURA, Minoru OKADA*, Malayappan SHRIDHAR* and John W. V. Miller*: Two- and Three-Dimensional Vision Systems for Inspection, Control, and Metrology KK, edited by Kevin G. Harding, Proceedings of SPIE Vol.5606, pp.19-pp.26, Bellingham, WA, 2004

Automatic Tracking for Regional Myocardial Motion by Correlation Method with Connecting Multiple ROIS, Wataru Ohyama, Masaki Inami, Tetsushi Wakabayashi, Fumitaka Kimura, Shinji Tsuruoka, Kiyotsugu Sekioka*: IEEJ Trans. EIS, Vol.124, No.10, 2004

Eigenspace Method by Autoassociative Networks for Object Recognition, Takamasa Yokoi, Wataru Ohyama, Tetsushi Wakabayashi and Fumitaka Kimura: Structural, Syntactic, and Statistical Pattern Recognition (Joint IAPR International Workshops SSPR2004 and SPR2004 Proceedings), Springer LNCS 3138, pp.95-103, Lisbon, Purtugal, Aug. 18-20, 2004

Two Dimensional Motion Tracking of Left Ventricular Myocardium Using Ultrasonic Doppler Signal, Wataru Ohyama, Toshikazu Muramatsu, Tetsushi Wakabayashi, Fumitaka Kimura, Shinji Tsuruoka and Kiyotsugu Sekioka*: Proceedings of the Sixth IASTED International Conference on Signal and Image Processing, pp.436-440 (#444-187), Honolulu, Hawaii, USA, Aug. 23-25, 2004

Local Slant Estimation for Handwritten English Words, Yimei Ding, Wataru Ohyama, Fumitaka Kimura and Malayappan Shridhar*: Proceedings of the 9th International Workshop on Frontiers in Handwritten Recognition, pp.328-333, Kokubunji, Tokyo, Japan, Oct. 26-29, 2004

A Study on Decision Rule for Japanese Dictation Test, Meng Shi, Wataru Ohyama, Tetsushi Wakabayashi and Fumitaka Kimura: Proceedings of the 9th International Workshop on Frontiers in Handwritten Recognition, pp.592-596, Kokubunji, Tokyo, Japan, Oct. 26-29, 2004

The Impact of OCR Accuracy on Automatic Text Classification, Guowei Zu, Mayo Murata, Wataru Ohyama, Tetsushi Wakabayashi and Fumitaka Kimura: Proc. of AWCC2004, ZhenJiang, China, pp.403-409, Nov. 2004

Accuracy Improvement of Automatic Text Classification Based on Feature Transformation and Multi-classifier Combination, Xuexian Han, Guowei Zu, Wataru Ohyama, Tetsushi Wakabayashi and Fumitaka Kimura: Proc. of AWCC2004, ZhenJiang, China, pp.463-468, Nov. 2004

Department of Physics Engineering

*nonmember

Fluctuation Spectrum of Director in Cholesteric Phase with External Field, M. Yamashita: Mol. Cryst. Liq. Cryst. 409, pp. 219-227, 2004.

Fluctuation spectrum of molecular orientation in the cholesteric phase exposed to the external field with positive anisotropy is calculated for the general case of Frank's elastic constants. The stability of the phase is certified in the meaning of Peierls-Landau theory.

The Order and the Polarisation of the System Composed of Polar Gay-Berne Molecules with Bend, T. Miyazaki* and M. Yamashita: Mol. Cryst. Liq. Cryst. 413, pp. 117-124, 2004.

NVT molecular dynamics simulation is carried out to study the relation of molecular shape and dipole moment to the liquid crystalline ordering at the system of coupled Gay-Berne molecules which are dimers of two types of Gay-Berne particles coupled by harmonic spring at each end. The appearances of polarization and biaxiality together with the location of clearing temperature are reported for various types of combination of position and direction of the dipole attached to molecule.

Ordering in Chiral Smectics at Freely Suspended Film, M. Yamashita: Ferroelectrics 309, pp. 63-73, 2004.

The method to study phase transitions of thin systems on the basis of the bulk phase diagram is applied to a freely suspended film of ferroelectric smectics showing a first order phase transition in the bulk, where the ordering effect due to surface layers is replaced by an effective field which is conjugate to the order parameter. In the framework of a phenomenological free energy, whose coefficients are determined form the experimental evidence about C7, behaviours of transition are clarified, which coincides with experimental findings, and especially the small shift of transition temperature from the bulk one is elucidated. The continuous change occurring in the system of thickness just below a critical thickness is proved to be achieved by an insertion of an unstable state of the interior layers, which is never realised in the bulk. This mechanism of continuous change shows the difference between the ordering effects due to the boundaries and external fields.

Isotropic, Nematic and Smectic A Phase Behaviour in a Fictitious Filed, M. Torikai and M. Yamashita: J. Phys. Soc. Jpn., 73, pp. 2154-2157, 2004.

Phase behaviours of liquid crystals under external fields, conjugate to the nematic order and smectic order, are studied within the framework of mean field approximation developed by McMillan. It is found that phase diagrams, of temperature vs interaction parameter of smectic A order, show several topologically different types caused by the external fields. The influences of the field conjugate to the smectic A phase, which is fictitious field, are precisely discussed.

Nematic Ordering of a Liquid Crystalline Homeotropic Cell, M. Yasen, M. Torikai and M. Yamashita: J. Phys. Soc. Jpn., 73, pp. 2453-2457, 2004.

Nematic ordering in a very thin system under the homeotropic anchoring condition is studied in the framework of the Maier-Saupe model. Nonuniformity due to the boundary effect is described in terms of an effective field which is conjugate to the order parameter, and behaviour of the system is analysed by observing loci of the effective fields on the phase diagram of the bulk. A continuous change occurring at the system with thickness just smaller than a critical thickness is shown to be mediated by an unstable state; a metastable high-temperature phase changes to a metastable low-temperature one continuously via an unstable phase between them. This mechanism is an analogue of the phenomenon occurring in a freely suspended film of a certain chiral smectic material.

Critical behavior near the metal-insulator transition in the one-dimensional extended Hubbard model at quarter filling, Kazuhiro SANO, Yoshiaki Ono* : Phys. Rev. B70, pp.155102-1--155102-6, 2004.

We examine the critical behavior near the metal-insulator transition (MIT) in the one-dimensional extended Hubbard model with the on-site and the nearest-neighbor interactions U and V at quarter filling using a combined method of the numerical diagonalization and the renormalization group(RG). The Luttinger-liquid parameter (K_r) is calculated with the numerical diagonalization for finite size systems and is substituted into the RG equation as an initial condition to obtain K_r in the infinite size system. This approach also yields the charge gap in the insulating state near the MIT. The results agree very well with the available exact results for U=infinity even in the critical regime of the MIT where the characteristic energy becomes exponentially small and the usual finite size scaling is not applicable.

Antiferromagnetic Exchange Coupling in RE-TM Films, Akira Inagaki, Masaya Tsuneoka, Atsushi Ohshima, Tadashi Kobayashi, Yuji Fujiwara, Shigeru Shiomi and Tsutomu Shiratori*: J. Magn. Soc. Jpn., 28, pp.312-317, 2004.

This paper reports the magnetic and magneto-optical properties of antiferromagnetic exchange coupled (AFC) RE-TM double layered films prepared by sputter deposition. The sample structure is glass/underlayer Ru/Gd-Fe-Co/(E-layer Fe-Co)/AFC layer Ru/(E-layer Fe-Co)/Gd-Fe-Co/protectivelayer Ru. The exchange coupling energy J was found to depend on Ru thickness of the AFC layer. The first AFC peak was found at an AFC layer thickness of 3.0 Å. Next we inserted a thin Fe-Co layer called the E-layer, between the AFC layer and the magnetic layer to improve the J value. In AFC RE-TM double layered films, a complicated Kerr loop was observed when each magnetic layer was thin. Then we compared the calculated result with the experimental result to distinguish the ferromagnetic coupling from the AFC. Next we investigated thermal stability of J.

Wall Structure and Energy on DWDD, Atsushi Ohshima, Kentaro Kusano, Tadashi Kobayashi, Yuji Fujiwara, Shigeru Shiomi and Masahiko Kaneko*: Trans. Magn. Soc. Jpn., 4, pp.152-155, 2004.

Wall structure and energy have been simulated for the Domain Wall Displacement Detection

(DWDD), and the front process and the rear process under temperature gradient have been considered. For the front process, when the mark length is comparable with the domain wall width in the displacement (D) layer, the domain copied on the D-layer from the memory layer collapses. By making the D-layer thin, the minimum mark length for which the domain wall displacement occurs can be shortened. For the rear process, we confirmed that by inserting the control layer between the D-layer and the switching layer, the mark length with which the ghost signal is suppressed becomes longer. By making the anisotropy energy constant in the D-layer increase, improvement in the DWDD process is expected.

Noncollinear magnetism phenomena induced at surface domain walls and in vortex cores of magnetic quantum dots, A. J. FREEMAN*, Kohji NAKAMURA, Tomonori ITO : Journal of Magnetism and Magnetic Materials 272-276, pp. 1122-1127, 2004.

We report noncollinear magnetism phenomena by means of several recent examples: (a) enhancement of magnetocrystalline anisotropy in ferromagnetic (FM) Fe films by intra-atomic noncollinear magnetism, (b) noncollinear magnetic structures of domain walls in FM Fe and antiferromagnetic NiMn, and (c) curling spin and orbital structures in the vortex core of an Fe quantum dot, as obtained from the first principles full-potential linearized augmented plane wave method including noncollinear magnetism with no shape approximation for the magnetization. These results are in good agreement with experiments, and give new information about magnetic phenomena at surfaces and in nanostructures.

Noncollinear magnetism and enhancement of magnetocrystalline anisotropy at the Σ3(111) grain boundary in ferromagnetic Fe, Kohji NAKAMURA, Tomonoi ITO, A. J. Freeman*, L. Zhong*, J. F. Castro* : Applied Physics Letters 84 , pp. 4974-4976, 2004.

Magnetic structures and magnetocrystalline anisotropy of the Σ3(111) grain boundary (GB) in ferromagnetic Fe are investigated by the first-principles full-potential linearized augmented plane-wave method including intra-atomic noncollinear magnetism. In breaking the spatial translation symmetry in a crystalline solid, GB is found to give rise to a magnetic noncollinearity, where the magnetic moments at both sides of the GB orient at a angle about 10° with respect to each other. Importantly, the presence of the GB enhances the magnetocrystalline anisotropy energy by one order of magnitude from its bulk value and may induce a pinning effect on the magnetization rotation or magnetic domain wall motion.

Atomically sharp magnetic domain wall in thin films Fe(110): A first principles noncollinear magnetism study, Kohji NAKAMURA,, Yoshifumi TAKEDA, Toru AKIYAMA, Tomonori ITO, A. J. Freeman* : Physical Review Letters 93, pp.057202-1-4, 2004.

Magnetic domain wall structures in an Fe(110) monolayer are determined by the highly precise firt principles full-potential linearized augmented plane-wave method including intra-atomic noncollinear magnetism. The self-consistent results demonstrate that the magnetization changes from one orientation to the opposite (180°) orientation within 8 Å width without any abrupt rotation. This

narrow domain wall is found to arise from band effects. Our results are consistent with and support domain walls having a 6 Å width recently observed in spin-polarized scanning tunneling microscopy experiments.

Magnetic structures and out-of-plane magnetic anisotropy at the exchange bias interface: Co/FeMn, Kohji NAKAMURA, Tomonori ITO, A. J. Freeman* : Physical Review B 70, pp. 060404(R)-1-4, 2004.

The magnetic structures and anisotropy at the compensated ferromagnetic/antiferromagnetic Co/FeMn interface are investigated by the highly precise first principles full-potential linearized augmented plane-wave method that incorporates intra-atomic noncollinear magnetism in order to understand the magnetic complexity involved in the spin-flop coupling and the presence of intra-atomic noncollinear magnetism. The self-consistent results predict that the Fe moments in the FeMn layer reorient away from their directions in bulk FeMn so as to be parallel to the Co moment direction – a reorientation that induces an out-of-plane magnetic anisotropy. These results appear to support and confirm recent experimental x-ray magnetic circular dichroism findings that rule out spin-flop coupling as the mechanism for exchange bias in this system.

Modern computational magnetism: role of noncollinear magnetism in complex magnetic phenomena, A. J. FREEMAN* and Kohji NAKAMURA: Physica Status Solidi (b) 241, pp. 1399-1405, 2004.

Modern computational magnetism continues to grow at an accelerating pace stimulated by new and exciting discoveries important for basic science and technological applications. Here, we review some recent important progress made in treating complex noncollinear magnetic phenomena arising from the breaking of symmetry at surfaces, interfaces, and nanostructures, by means of our newly generalized first principles full-potential linearized augmented plane wave (FLAPW) method for noncollinear magnetism with no shape approximation to the magnetization. Because of space limitations, we restrict our report illustrate results of the noncollinear magnetic structures induced at the FM NiFe/AFM NiMn interfaces, in the domain walls of FM Fe and AFM NiMn, and in the vortex cores of a Fe quantum dot. These results are in good agreement with experiments and give new information about magnetic phenomena at surface, interfaces, and in nanostructures.

Systematic theoretical investigations of adsorption behavior on the GaAs(001)-c(4x4) surfaces, Tomonori ITO, Kazumi TSUTSUMIDA, Kohji NAKAMURA, Yoshihiro KANGAWA*, Kenji SHITRAISHI*, Akihito TAGUCHI*, Hiroyuki KAGESHIMA* : Applied Surface Science 237, pp. 194-199, 2004.

Adsorption behavior on the GaAs(001)-c(4x4) surfaces is systematically investigated by using our ab initio-based approach and the Monte Carlo methods. The change in stable structure of the c(4x4) surfaces is clarified by considering adsorption or desorption of surface dimers as functions of temperature and As pressure. The calculated results imply that the c(4x4) surface with As dimers is stable at low temperatures less than ~400 K, whereas the surface with Ga-As dimers is stabilized at high temperatures in the range of ~400 K to ~700 K. The disordered dimer arrangements consisting of Ga and As substituted by each other in the c(4x4) unit cell hardly appear even at high temperatures

such as ~800 K. We also investigate the behavior of Ga and As adatoms on these c(4x4) surfaces. The calculated results reveal that Ga atoms can adsorb and migrate on the surfaces while desorption of As adatoms proceeds without sufficient migration.

Theoretical investigations of adatom behavior on non-planar surfaces with GaAs(*n*11)A, Koichi ASANO, Yoshihiro KANGAWA*, Hirotoshi ISHIZAKI, Toru AKIYAMA, Kohji NAKAMURA, Tomonori ITO : Applied Surface Science 237, pp. 206-212, 2004.

The behavior of Ga and As adatoms on non-planar surfaces consisting of GaAs(001)-(2x4) and GaAs(*n*11)A (*n*=2, 3 and 4) surfaces are investigated by empirical interatomic potentials with the aid of ab initio calculations. The calculated results imply that Ga adsorption energies strongly depend on the surface orientation, whereas As adsorption energies keep almost constant. The difference in adsorption energies can be interpreted by considering strain energy. In particular, Ga adatom is stabilized on the (311)A surface by the smallest strain energy forming interatomic bonds with three As atoms located at the regular fcc sublattice. Furthermore, we roughly simulate resultant surface profile of GaAs thin films on the non-planar surfaces consisting of the (001)-(2x4) top and (*n*11)A side surfaces based on the rate equation. The simulated results reveal that the non-planar surface with (311)A side surface forms the linear surface profile.

First-principles analyses of O_2 molecules around ultrathin SiO_2/Si(100) interface, Toru AKIYAMA, Hiroyuki KAGESHIMA*, Tomonori ITO : Japanese Journal of Applied Physics 43, pp. 7903-7908, 2004.

The microscopic structures and reaction mechanisms of O_2 molecules at ultrathin SiO_2/Si(100) interface are investigated based on first-principles total-energy calculations. It is found that the molecular-type oxygen is stable in the SiO_2 region of the interface, while the O_2 in the Si substrate dissociates and two Si-O-Si bonds are formed. It is also found that the O_2 in the SiO_2 region can directly react with the Si substrate. The energy barrier for its reaction (0.2 eV) does not correspond to (previously consented) serving process of interfacial Si-Si bonds, but to the formation of weak Si-O bonds between the O atoms of oxidant and the interfacial Si atoms: The hybridization of the oxygen-2p orbitals of the oxidant and the valence band states of the Si substrate is the principal factor of the reaction. The calculated results imply that other microscopic mechanisms such as accumulation of interfacial strain or its release mechanisms are involved in the interfacial reaction during Si oxidation.

Theoretical study of excess Si emitted from Si-oxide/Si interface, Hiroyuki KAGESHIMA*, Masashi UEMATSU*, Kazuto AKAGI*, Shinji TSUNEYUKI*, Toru AKIYAMA, Kenji SHIRAISHI* : Japanese Journal of Applied Physics 43, pp. 8223-8226, 2004.

The excess Si emitted from the Si-oxide/Si interface is studied using the first-principles calculations. It is shown that the excess Si can have many (meta-) stable positions around the interface. In addition, some positions in the oxide do not have any dangling bonds or floating bonds in contrast to those in the bulk crystalline Si. The results indicate that the emitted Si can be located in the oxide layer

but they do not necessarily cause charge traps in the oxide. The emitted Si atoms are thought to just be oxidized and absorbed into the oxide while a portion of them cause the E' centers, the P_b centers or charge traps.

Thermodynamic stability for group IV alloy semiconductors [in Japanese]. Tomonori ITO, Yoshihiro KANGAWA* : Journal of the Japanese Association for Crystal Growth 31, pp. 4-11, 2004.

Thermodynamic stability of group IV alloy semiconductors such as $Si_{1-x-y}Ge_xC_y$ solid solutions in bulk and thin film states is systematically investigated by excess energy calculations based on empirical interatomic potentials and Monte Carlo (MC) simulations. In bulk state, the calculated excess energies for $Si_{1-x-y}Ge_xC_y$ have positive values over the entire concentration range. This implies that $Si_{1-x-y}Ge_xC_y$ with a random distribution of Si, Ge and C is thermodynamically unstable at 0 K. Furthermore, the excess energies of $Si_{1-x-y}Ge_xC_y$ increase with Ge content x when C content y remains constant. This is because an increase of Ge content introduces large strain energy in $Si_{1-x-y}Ge_xC_y$. In thin film state, although lattice constraint at the interface reduces the excess energies by 20-30 % of those in bulk state, we obtain similar results to those in bulk state. Further MC simulation reveal that Ge atoms segregate in the topmost layer and C atoms accumulate in the second layer.

Plastic Deformations of Micro-Spheres by Solidified Lubricants and Lubricants' Shear Characteristics under Very High Pressure (Part 1) — Observation of Plastically-Deformed Micro-Spheres — [in Japanese], Yuichi NAKAMURA, Yutaka ISHIBASHI* and Yasushi KUROSAKI: Tribologist, 49-6, pp. 518-524, 2004.

Fractal analysis of adhesion on tool surface in compression of aluminum strips by using AFM [in Japanese], Masahito MATSUI, Yasushi KUROSAKI and Yusuke MIYAUCHI: Journal of Japan Institute of Light Metals, 54-1, pp. 9-13, 2004.

Adhesion properties in simple compression of aluminum strips are analyzed in the micro/nanometer range by employing the zeroset and power spectrum fractal analyses. An atomic force microscope (AFM) is used to estimate the fractal dimensions. It is found that the adhesion and tool and specimen surfaces have fractal structure. Various fractal dimensions obtained for the adhesion and tool and specimen surfaces are compared to each other and discussed. When the surface roughness of tool is same, the ratio of the total adhesion area depends on the fractal dimension. Though the AFM apparatus is difficult to distinguish the adhesion particles from the tool surface, the power spectrum dimension has possibility of distinguishing the adhesion particles from the tool surface. Finally, a method for computer simulation of the nanometer scale surface structure is presented, and satisfactory images are constructed.

Nanofractal Analysis on Material Surfaces Using AFM, Mir Behdad Khamesee, Yasushi Kurosaki, Masahito Matsui and Kenichi Murai: Materials Transactions, 45-2, pp. 469-478, 2004.

The surface structures of four materials (a pure aluminum sheet, an aluminum alloy sash, a

thickness gauge and a magnetic tape) are observed on the nanometer scale by atomic force microscopy (AFM) and analyzed by one-dimensional fractal analyses. It is confirmed for all the surfaces that they have a self-affined fractal property under a resolution of 1nm. The two-dimensional fast Fourier transformation (2D-FFT) analysis is also applied to these surfaces and their characteristics are clarified. The power spectrum model for surface simulation is proposed and its validity is confirmed by experimental results. A method for simulating surface structure of any materials is presented, and its validity is shown on some materials whether in-plane isotropic or anisotropic. A computer aided engineering (CAE) system composed of 2D-FFT and inverse FFT (IFFT) for quantitative estimation of surface nanostructures is advanced and applied to various surface problems. It enables the mass data of material surface to compress into only three parameters.

Abstracts of Books and Reviews (2004)

Department of Mechanical Engineering

* nonmember

Introduction of probability and statistics, Yoshihiko Nomura: Corona Publishing Co. LTD. 2004

Fundamental issues on probabilities and statistics are described. It starts from explaining such fundamental concepts as permutations and combinations, conditional probability, Bayes' theorem, mean, and variance. Then, it introduces some fundamental probability distributions such as the Binomial distribution, the Poisson distribution, the normal distribution, the chi-square distribution, Student's t distribution, the Fisher's F distribution. Based on these probabilistic subjects, some important statistical subjects are described such as the unbiased estimation, the interval estimation, the tests of hypotheses, and the curve fitting and correlation. As for the test, there are described procedures of testing such statistical values as the population mean, the difference of means, the ratios of variances, and the analysis of variance including one factor and two factor experiments.

Problems in Control Engineering, Norihiko Kato: Japan Society of Mechanical Engineers, pp.63-92 and 119-130, June, 2004

This book is written for the exercise of the control engineering. In chapter 8, the state space representation of dynamic system is introduced. The solution of state equation, the relation to the transfer function and the connection of the systems are described. In chapter 9, coordinate transformation and the meaning are explained. Because the representation of the system is not unique, we can transform the system to analyze easily. In chapter 10, to design control system, controllability and observability are introduced and the examine methods of them are shown. Structure of the system is discussed and the canonical decomposition is described. As appendix, the formulae of the linear algebra and the ordinary differential equation are summarized.

Jet Flow Engineering - Fundamentals and Application –, Toshihiko SHAKOUCHI: Morikita Shuppan Co., 2004.

This book shows the fundamentals of jet flow, for example, flow characteristics and flow structure of various kinds of jet flows and the practical industrial applications. The contents are as follows.

Ⅰ. Fundamentals of Jet Flow Engineering

1.Fluid Dynamics of Jet Flow 2.Computational Fluid Dynamics for Jet Flow 3.Free and Wall Jet Flows 4.Attached Jet Flow 5.Impinging Jet Flow 6.Stability of Jet Flow and Oscillatory Phenomena 7.Mixing and Diffusion of Jet Flow and Their Control

Ⅱ. Application of Jet Flow Engineering

8. Application of Impinging Jet Flow 9.Application of Mixing and Diffusion of Jet Flow 10.High Speed Liquid Jet Flow 11.Multiphase Jet Flow, Buoyant and Plume Jet Flows, and Gas-Liquid Two-Phase Jet Flow 12.Multiphase Jet Flow, Gas-Solid Two-Phase Jet Flow

Department of Electrical and Electronic Engineering

* nonmember

Guide Book for Introduction to Electron Microscopy, Akinori OHSHITA: Japanese Scientific Societies Press, pp.139-155, August, 2004

This book is a guide for introduction to electron microscopy.

Basic of OFDM Technique and Its Applications (Book), Hideo KOBAYASHI: Triceps, pp.1-190, May 2004. [in Japanese]

A survey of relationship between learners' confidence in answers and their reviewing of incorrect answers [In Japanese], Shinobu TABATA and Hidehiko KITA: Research Reports of the Common Education, Mie University, Vol.12, pp.39-41, 2004

A questionnaire survey of relationship between learners' confidence in answers and their reviewing of incorrect answers [In Japanese], Shinobu TABATA, Hidehiko KITA, Terumine HAYASHI and Tsutomu SHIMOMURA: Research Reports of the Faculty Engineering, Mie University, Vol.29, 2004

Controls of a-c Orientation Growth of YBCO Thin Film crystals for YBCO/Ferro Double Layered Tunable Microwave Filters, Tamio ENDO, Kouji YOSHII, Takahisa SAKURADA, Michi OGATA, Ajay SARKAR, Masanori OKADA, Hidetaka NAKASHIMA: Proc. Int. Workshop on Crystal Growth and Characterization of Technologically Important Materials (Chennai, 2004), pp.89-111, 2004

Fundamentals and applications of carbon nanotubes [in Japanese], Edited by Riichiro SAITO and Hisanori SHINOHARA, *Baifu-kan Co., Ltd* (Mar. 31, 2004) pp320 Koichi HATA and Yahachi SAITO* (co-written: Contributed to Chapter 11, pp. 159-169)

Field emission property of carbon nanotubes and its application to electron emitters are described.

Field emission display technology –Present and prospect of next generation display FED [in Japanese], Edited by Yahachi SAITO, CMC Publications (June 2004) pp.218 Koichi HATA and Yahachi SAITO* (Co-written: Contributed to Chapter 2, pp.39-48)

Field emission property of carbon nanotubes and its application to cathode materials used in field emission displays (FEDs) are described.

Department of Chemistry for Materials

* nonmember

Synthesis of Organic Compounds V [in Japanese], Makoto SHIMIZU: The Fifth Series of Experimental Chemistry, Vol. 17, Maruzen (Tokyo), pp. 311-336, 2004

Synthesis of Organic Compounds VI [in Japanese], Makoto SHIMIZU, Iwao HACHIYA: The Fifth Series of Experimental Chemistry, Vol. 18, Maruzen (Tokyo), pp. 280-310, 2004

Synthesis of Organic Compounds VII [in Japanese], Makoto SHIMIZU: The Fifth Series of Experimental Chemistry, Vol. 19, Maruzen (Tokyo), pp. 160-171, 2004

MgX, MgOR, MgN, etc, Makoto SHIMIZU: In “Science of Synthesis / Houben-Weyl”, Vol. 7, Georg Thieme Verlag (Stuttgart), pp. 629-667, 2004

Antigen-Based B Cell Targeting Technique to Generate High Yields of Monoclonal Antibodies, Masahiro TOMITA, Mitsumi SUGAO, Takanobu TANIGUCHI, Jun-ichiro TANAKA, Hana SAWADA*, Shigeru FUJIMOTO*, Norikazu NISHINO*, Tian Yow TSONG*, Tetsuro YOSHIMURA: Human Antibodies,13, p.42, 2004

Dynamics of an Air Bubble Rising in a Hele-Shaw Cell Filled with Polymer Solutions [in Japanese], Sukehiro NIGA, Nobuaki GOH, Masami KAWAGUCHI: Polymer Processing 53 (6), pp. 274-277, 2004

The buoyancy-driven paths of an air bubble rising in a Hele-Shaw cell, which contains aqueous polymer solutions, were described in terms of path instabilities, such as changes in the shape and trajectory of the bubble. An increase in the polymer concentration induced three path instabilities and in particular, a trajectory transition from a damped path to a straight one almost occurred at the same bubble diameter, irrespective of the polymer solution, due to the presence of Karman’s vortex-street.

Classification, Preparation, and Stabilization of Emulsions [in Japanese], Masami KAWAGUCHI: Modern Technology of Emulsification, Jyohohkikoh (Tokyo), Chapter 3, pp. 51-64, 2004

The basic experiments in emulsions were described in terms of the experimental procedure, classification, characterization, and applications of emulsions. In this chapter, some details for experimental estimation of the stability of emulsions were explained based on the characteristics of emulsions.

Rheology of Emulsification [in Japanese], Masami KAWAGUCHI: Rheology, Jyohohkikoh (Tokyo), Section 3, pp. 70-81, 2004

Rheological properties of emulsions were described in terms of emulsions stabilized by polymeric surfactants, emulsions depleted by polymers, and emulsions stabilized by silica particles coated with polymers. In this section, we emphasized that the stabilities of emulsions were strongly related with their rheological properties.

Department of Architecture

* nonmember

Conservation and Eco-City, Satoshi ASANO; “Regional Environmental Design and Succession” [in Japanese], Architectural Institute of Japan Edition, Shokokusha Published Ltd., pp.168-172, 2004

Machizukuri Practical Learning, Satoshi ASANO; “Machizukuri Learning” [in Japanese], Architectural Institute of Japan Edition, Maruzen Published Ltd., pp.34-44, pp.94-95. pp.104-111, 2004

Building Performance in Building Project Planning, Hiroyuki Takai; “Building Project Planning in Management Era” [in Japanese], Gihoudo Shuppan, pp.103-116, 2004

Super High-rise condominiums; Hiroyuki Takai and Taiichi Chikuma; “The Design of Modern Apartments Houses” [in Japanese], Shokokusha Publishing Co., pp.46-47, 2004

Common Spaces, Facilities and Services of Super High-rise condominiums [in Japanese], Hiroyuki Takai, Condominium Living, No.20, pp.30-33, 2004

Properties of Hardened Concrete [in Japanese], Chap.1 (Concrete Under Compressive Load), Shigemitsu HATANAKA, edited by Yasuo TANIGAWA*, Cement Journal Co., Ltd., pp.9-33, 2004.10

Fluidity and Prediction of Fresh Concrete[in Japanese], Chap.1 (Rheology Model and Various Measuring Methods), Naoki MISHIMA, edited by Yasuo TANIGAWA*, Cement Journal Co., Ltd., pp.9-33, 2004.9

Generation of structural shape by means of a multiobjective genetic algorithm,Toyofumi TAKADA and Keigo MATSUSHIMA, Book of Abstracts of the Int. Workshops on Advances in Computational Mechanics,p.104, 2004

Department of Physics Engineering

* nonmember

Quantum Mechanics—Revised Version—[in Japanese], Y. Abe: Mie University Press, Mie, 2004.

The contents are divided into four sections. The first section entitled "Fundamental Structure of Quantm Theory" consists of explanation on "Experimental Background" and "Discussion of Measurement", *etc.*. The second section entitled "Canonical Quantization and Equation of Motion" consists of explanation on "Schreudinger Theory" and "Heisenberg Theory", *etc.*. The third section entitled "Quantized System in Stationary States" consists of explanation on "Harmonic Oscillator" and "Hydrogen Atom", *etc.*. The forth section entitled "Approximation Methods" consists of explanation on "Perturbation Theories" and "Semiclassical Approximation", *etc.*.